Earth Sciences Scholarship Earth Sciences

6-27-2007

Chemical data assimilation estimates of continental U.S. ozone and nitrogen budgets during the Intercontinental Chemical Transport Experiment-North America

R B. Pierce
NOAA

T Schaack
University of Wisconsin-Madison

J Al-Saadi
NASA

T D. Fairlie
Harvard University

Chieko Kittaka
NASA

See next page for additional authors

Follow this and additional works at: https://scholars.unh.edu/earthsci_facpub

Part of the Atmospheric Sciences Commons

Authors

R B. Pierce, T Schaack, J Al-Saadi, T D. Fairlie, Chieko Kittaka, Gretchen Lingenfelser, M Natarajan, J R. Olson, Amber Soja, Tom Zapotocny, A Lenzen, M A. Avery, James Stobie, Donald Johnson, Melody A. Avery, G W. Sachse, A M. Thompson, Ronald C. Cohen, Jack E. Dibb, J Crawford, Didier Rault, Randall Martin, Jim Szykman, and Jack Fishman

Chemical data assimilation estimates of continental U.S. ozone and nitrogen budgets during the Intercontinental Chemical Transport Experiment–North America

Robert B. Pierce,[1] Todd Schaack,[2] Jassim A. Al-Saadi,[1] T. Duncan Fairlie,[1]
Chieko Kittaka,[1] Gretchen Lingenfelser,[1] Murali Natarajan,[1] Jennifer Olson,[1]
Amber Soja,[1] Tom Zapotocny,[2] Allen Lenzen,[2] James Stobie,[3] Donald Johnson,[2]
Melody A. Avery,[1] Glen W. Sachse,[1] Anne Thompson,[4] Ron Cohen,[5] Jack E. Dibb,[6]
Jim Crawford,[1] Didier Rault,[1] Randall Martin,[7] Jim Szykman,[8,9] and Jack Fishman[1]

[1] Global ozone analyses, based on assimilation of stratospheric profile and ozone column measurements, and NOy predictions from the Real-time Air Quality Modeling System (RAQMS) are used to estimate the ozone and NOy budget over the continental United States during the July–August 2004 Intercontinental Chemical Transport Experiment–North America (INTEX-A). Comparison with aircraft, satellite, surface, and ozonesonde measurements collected during INTEX-A show that RAQMS captures the main features of the global and continental U.S. distribution of tropospheric ozone, carbon monoxide, and NOy with reasonable fidelity. Assimilation of stratospheric profile and column ozone measurements is shown to have a positive impact on the RAQMS upper tropospheric/lower stratosphere ozone analyses, particularly during the period when SAGE III limb scattering measurements were available. Eulerian ozone and NOy budgets during INTEX-A show that the majority of the continental U.S. export occurs in the upper troposphere/lower stratosphere poleward of the tropopause break, a consequence of convergence of tropospheric and stratospheric air in this region. Continental U.S. photochemically produced ozone was found to be a minor component of the total ozone export, which was dominated by stratospheric ozone during INTEX-A. The unusually low photochemical ozone export is attributed to anomalously cold surface temperatures during the latter half of the INTEX-A mission, which resulted in net ozone loss during the first 2 weeks of August. Eulerian NOy budgets are shown to be very consistent with previously published estimates. The NOy export efficiency was estimated to be 24%, with NOx + PAN accounting for 54% of the total NOy export during INTEX-A.

Citation: Pierce, R. B., et al. (2007), Chemical data assimilation estimates of continental U.S. ozone and nitrogen budgets during the Intercontinental Chemical Transport Experiment–North America, *J. Geophys. Res.*, *112*, D12S21, doi:10.1029/2006JD007722.

1. Introduction

[2] During July and August, 2004 NASA conducted the Intercontinental Chemical Transport Experiment–North America (INTEX-NA) as part of the International Consortium for Atmospheric Research on Transport and Transformation (ICARTT) study. One of the key scientific goals of the 2004 phase of INTEX-NA is to quantify and characterize the inflow and outflow of pollution over North America [*Singh et al.*, 2006]. The effects of regional air quality, over the United States and elsewhere, on the global atmosphere become particularly important as world population increases require increases in agricultural production and continued economic growth leads to increased fossil fuel combustion [*Stevenson et al.*, 2006]. Combustion leads to anthropogenic emissions of CO2, CO, NOx (NO + NO2), SO2, and nonmethane hydrocarbons (NMHC) as well as particles that can significantly perturb the global atmosphere. In addition

---

[1]NASA Langley Research Center, Hampton, Virginia, USA.
[2]Space Science and Engineering Center, University of Wisconsin, Madison, Wisconsin, USA.
[3]Science Applications International Corporation, Washington, D. C., USA.
[4]Department of Meteorology, Pennsylvania State University, University Park, Pennsylvania, USA.
[5]Department of Chemistry, University of California, Berkeley, California, USA.

[6]Earth Sciences Department, University of New Hampshire Durham, New Hampshire, USA.
[7]Department of Physics and Atmospheric Science, Dalhousie University, Halifax, Nova Scotia, Canada.
[8]U.S. Environmental Protection Agency, Raleigh, North Carolina, USA.
[9]Now at NASA Langley Research Center, Hampton, Virginia, USA.

to these primary pollutants, secondary pollutants can have significant impacts on global tropospheric chemistry. In particular, the abundance and distribution of O3 governs the oxidative capacity of the troposphere. The global distribution of NOx, which is the critical limiting precursor for O3 production, is highly variable and is dependent on local photochemical loss and cycling processes involving NOx reservoir species (e.g., PAN, HNO3) as well as the magnitude of various sources which include transport from the stratosphere, natural emissions (lightning, soils, biomass burning) and anthropogenic emissions (industrial, aircraft, ships).

[3] This study focuses on estimating ozone and NOy (NOy = NO + NO2 + NO3 + HNO3 + HNO4 + 2*N2O5 + ClNO3 + PAN + organic nitrates) budgets over the continental U.S. and export to the global atmosphere. The approach we use is an Eulerian budget analysis as described by *Pierce et al.* [2003] and focuses on characterization of the relative contributions of (1) ozone and NOy sources and sinks within the continental U.S. domain and (2) regional to global exchange of ozone and NOy. There is compelling observational and modeling evidence of the link between continental U.S. emissions and the global atmosphere. *Knapp et al.* [1998] observed enhanced ozone (90–130 ppbv) just above the boundary layer over Cape Sable Island, Nova Scotia during the 1993 North Atlantic Regional Experiment (NARE). Back trajectory analysis indicated that these air masses had origins over the heavily industrialized N. E. United States. Model studies show episodic but significant remote influences from North America [*Jacob et al.*, 1993; *Wild et al.*, 1996; *Atherton et al.*, 1996; *Liang et al.*, 1998; *Li et al.*, 2004], particularly in the upper troposphere. This remote influence is driven by export of NOx or PAN, which thermally decomposes to NOx and leads to further in situ ozone formation [*Chameides et al.*, 1992]. Model-based estimates of NOy export efficiency suggest that 20–30% of the NOx emitted from the continental United States is exported to the global atmosphere as NOy [*Kasibhatla et al.*, 1993; *Horowitz et al.*, 1998, *Liang et al.*, 1998, *Li et al.*, 2004]. Observational estimates of continental U.S. NOy export suggest efficiencies ranging from 10–15% [*Parrish et al.*, 2004].

[4] The preceding discussion illustrates the uncertainties that arise because of complex interactions between highly heterogeneous surface emissions, local radical chemistry, boundary layer exchange processes, enhancements in background levels of O3 and its precursors, and long-range transport that ultimately determine the links between regional emissions and the global atmosphere. These links occur across multiple scales in both time and space and therefore require a unified approach, utilizing contemporaneous satellite and in situ observations, as well as model estimates of the chemical state of the atmosphere. Field missions such as INTEX-A, which use chemical model forecast guidance to optimize synergy between in situ sampling by airborne platforms and contemporaneous satellite composition measurements for both satellite validation and science studies, are an example of this unified approach. However, an "optimized combination" of satellite, in situ observations, and model estimates is best accomplished through chemical data assimilation. Data assimilation provides a physically consistent representation of the observed atmospheric state and involves blending information from different sources and different times to yield a best estimate, or "analysis" at a particular time. Models play an important role in data assimilation by providing an estimate, or "first guess" of the current fields based on previous analyses. The analysis is constructed by applying an "analysis increment" to the model first guess. The analysis increment is determined through variational approaches that minimize the differences between the observation and first guess under constraints that are determined by the relative errors in the respective fields [*Errico*, 1999].

[5] For the current study we utilize ozone analyses (constrained with assimilated satellite measurements) and NOy predictions from the Real-time Air Quality Modeling System (RAQMS) [*Pierce et al.*, 2003] to estimate the ozone and NOy budget over the continental United States. The manuscript is organized as follows: Section 2 provides an updated description of the RAQMS, which has undergone significant revisions since *Pierce et al.* [2003]. Section 3 focuses on evaluation of the model O3 analysis as well as CO, NOy, and net O3 production, defined as production-loss (P-L) predictions based on comparisons with satellite, ozonesonde, airborne, and ground based measurements. Section 4 discusses the contributions to ozone and NOy in the troposphere and lower stratosphere due to stratosphere-troposphere exchange processes during INTEX-A. The continental U.S. ozone and NOy budgets during INTEX-A are presented in section 5. Section 6 includes a discussion focusing on the interpretation of the INTEX-A results in light of previous studies. Section 7 provides a summary and conclusions.

2. Model Description

[6] The chemical modeling/assimilation tool used in this study is the NASA Langley Research Center/University of Wisconsin (LaRC/UW) Real-time Air Quality Modeling System (RAQMS). RAQMS is a portable, global- to regional-scale meteorological and chemical modeling system which has been developed for assimilating remote observations of atmospheric chemical composition and predicting regional air quality within any region of the planet Earth [*Pierce et al.*, 2003]. This study focuses on the global modeling/assimilation component of RAQMS. The UW hybrid isentropic coordinate model [*Schaack et al.*, 2004] is the dynamical core for the global component of RAQMS. *Zapotocny et al.* [1996, 1997a, 1997b] established that hybrid isentropic coordinate models simulate processes involving the long-range transport of trace constituents to a higher degree of accuracy than other existing global models.

[7] During INTEX-A RAQMS provided daily 4 day 2 × 2.5° global chemical forecasts, initialized with ozone analysis based on real-time assimilation of TOMS V8 ozone column data, to assist in flight planning. The daily assimilation/forecast cycle consisted of a series of 6 hour online chemical/dynamical forecasts, initialized with NOAA GFS meteorological analyses at 1200 UT, 1800 UT, 0000 UT, and 0600 UT. At the end of each 6 hour forecast, the ozone distribution was reinitialized on the basis of the RAQMS TOMS V8 assimilation. After 24 hours of assimilation, a 4-day online chemical/dynamical forecast was begun. For

the current study, we conducted a post mission 1.4 × 1.4 "reanalysis" from 1 July to 15 August 2004, with meteorological field initialized from the GFS analyses every 6 hours and including stratospheric ozone profile assimilation in addition to the TOMS column assimilation. The assimilation of stratospheric ozone profiles provides observational constraints on the lower stratospheric ozone in the reanalysis and significantly reduces biases relative to ozonesonde and in situ ozone measurements in the upper troposphere/lower stratosphere.

2.1. RAQMS Unified Stratosphere/Troposphere Chemistry

[8] The RAQMS unified stratosphere/troposphere chemistry module has been developed to represent photochemical processes governing ozone formation and destruction within Earth's atmosphere from the surface to about 60 km. The chemical formulation follows a family approach with partitioning based on photochemical equilibrium approximations. Continuity equations are solved for 55 families and individual constituents and by determining equilibrium concentrations of 86 separate species. The standard Ox-HOx-NOx-ClOx-BrOx cycles governing the formation and destruction of odd oxygen, tropospheric NOx-HOx reactions, oxidation of CH4 and CO are considered [*Pierce et al.*, 2003]. Recent updates include an extended carbon bond scheme for oxidation of nonmethane hydrocarbons (NMHC) and explicit treatment of isoprene oxidation. Photochemical tendencies are calculated with a quasi-steady state approximation based on exact solution of the continuity equation. Kinetic rates and photolytic quantum yields and absorption cross sections are from *Sander et al.* [2003] with the $N2 + O(^1D)$ quenching rate from *Ravishankara et al.* [2002]. Photolytic rates are calculated using the Fastj2 method [*Bian and Prather*, 2002]. Stratospheric heterogeneous reactions on liquid aerosol [*Carslaw et al.*, 1995] and polar stratospheric cloud [*Chipperfield*, 1999] surfaces are considered.

[9] The NMHC chemical scheme is based on the lumped structure approach of the Carbon Bond–IV mechanism (CB-IV) [*Gery et al.*, 1989] with adjustments necessary for large-scale (regional or global) application as presented by *Zaveri and Peters* [1999] (henceforth called CB-Z). Additional extensions implemented in the LaRC unified chemistry include an improved isoprene oxidation scheme and the semiexplicit treatment of propane. The resulting NMHC formulation can be summarized as follows: C2H6 (ethane), C2H4 (ethene) and CH3OH oxidation are treated explicitly; C4 and larger alkanes and C3 and larger alkenes are lumped via a carbon bond approach as updated in *Zaveri and Peters* [1999], with lumped groups for species such as aldehydes, ketones, peroxides and organic nitrates; C3H8 (propane) is handled semiexplicitly, i.e., C3H8 and its corresponding peroxy radicals are tracked explicitly (as by *Sander et al.* [2003] and *Kirchner and Stockwell* [1996]) while other oxidation products such as peroxides and aldehydes are lumped into the appropriate species following the carbon bond approach for higher alkanes; and isoprene is modeled after the Carter four-product mechanism as modified for RADM2 [*Carter*, 1996]. Aromatic chemistry

is not included. Concentrations of 2 species, acetone and methanol, are currently specified according to climatologies.

[10] The replacement of the CB-Z isoprene oxidation scheme with a more detailed four-product mechanism allows more accurate representation of PAN, which is an important nitrogen reservoir species. The four-product mechanism explicitly represents the major identified secondary isoprene oxidation products methacrolein (MACR), methyl vinyl ketone (MVK) and peroxymethacryloyl nitrate (MPAN). Rate constants, products and yields have been updated as reported in the literature [e.g., *Orlando et al.*, 2002].

[11] Climatological emissions of NOx and CO include anthropogenic and natural sources and are based largely on 1 × 1° public databases available from GEIA/EDGAR with updates for Asian emissions from *Streets et al.* [2003] and additional biogenic CO sources as described by *Duncan and Bey* [2004]. Aircraft NOx emissions are obtained from the HSRP database [*Stolarski et al.*, 1995]. Lightning NOx emissions are calculated on the basis of *Price et al.* [1997] using instantaneous convective cloud heights, and are distributed in the vertical according to *Pickering et al.* [1998]. Biomass burning emissions of NOx are scaled to those of CO with emission factors (NOx/CO) that vary from [0.0256 to 0.0174] depending on ecosystem type. As will be shown, total NOx emissions (transportation, industrial, aircraft, biomass, soil, and lightning) over the continental United States during INTEX-A study period (1 July to 15 August 2004) is equal to 0.94 Tg N, with lightning emissions accounting for 0.16 Tg N of this total. The EPA 2002 National Emission Inventory (NEI) NOx emission inventory (excluding lightning) is 5.855 Tg N/year resulting in 0.74 Tg N during the study period, which is within 5% of our nonlightning NOx emissions. *Hudman et al.* [2007] conducted GEOS-CHEM NOx emission sensitivity studies during INTEX-A using two different NOx emission inventories. The baseline inventory used EPA 1999 National Emission Inventory (NEI99) version 1 and resulted in total NOx emissions during the INTEX-A study period of 1.17 Tg N, with lighting emissions accounting for 0.068 Tg N. A second emission inventory, which included 50% reductions in industrial and a factor of 4 increase in lightning NOx emissions, resulted in 1.2 Tg N emissions during the study period. The NEI99 and top-down NOx emission inventories used by GEOS-CHEM are 24% and 27% higher than the GEIA/EDGER emission inventory used for the RAQMS simulations, respectively. Emissions of NMHC species are generally based on the GEIA database. Surface sources of N2O, CH4, and halocarbons are implicitly assumed by imposing a constant mixing ratio at the surface appropriate for 1990 [*World Meteorological Organization*, 1993]. Surface deposition is computed according to the surface type and drag coefficients, with the calculation of the deposition rate modeled after *Galbally and Roy* [1980] and *Levy et al.* [1985]. Dry deposition is computed for O3, peroxides, aldehydes, NO2, CO and nitric acid using deposition velocities from *Muller and Brasseur* [1995]. Online wet removal of soluble species is based on convective fluxes and precipitation amounts [*Liu et al.*, 2001; *Park et al.*, 2004]. Tropospheric heterogeneous
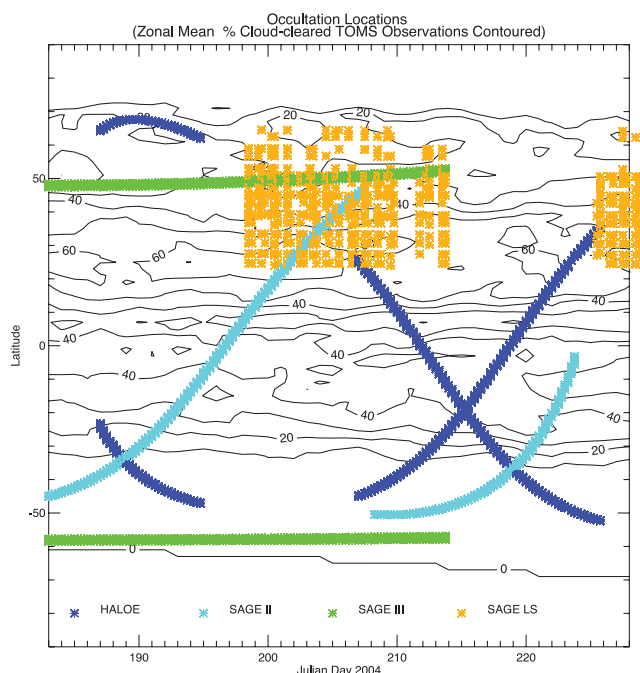
Figure 1. Latitude-time series of the location of observations used in the RAQMS assimilation. Symbols indicate the latitude of solar occultation and limb scattering observations. Contours indicate the density (% of total at each latitude) of cloud-cleared total column measurements.

loss of N_2O_5 is based on zonal averaged rates from *Dentener and Crutzen* [1993].

2.2. RAQMS Ecosystem-Based Wild Fire Emission Inventory

[12] Alaskan and Canadian wild fires had a significant impact on North American chemical composition during INTEX-A. The RAQMS biomass burning emissions for Alaska and Canada use an ecosystem-based approach developed by *Soja et al.* [2004] to predict total direct carbon emissions. *Soja et al.* [2004] used a spatially and temporally explicit model that incorporated a satellite-based (AVHRR) fire database and ecoregion-specific carbon consumption estimates for three classes of severity to estimate a range of total direct carbon and trace gas emissions from fires in Siberia from 1998 through 2002. We have extended this algorithm to North America using MODIS thermal anomaly data to provide area burned estimates. Briefly, the approach is as follows: (1) Static carbon consumption estimates for low-severity surface fires, medium-severity fires, and high-severity fires are based on the amount of carbon contained in individual ecosystems [*Olson*, 1983; *Zinke et al.*, 1986]. (2) Daily $1 \times 1°$ North American area burned estimates are obtained using MODIS thermal anomaly products. (3) On the basis of carbon consumption and area burned, daily total direct carbon emissions from fire events in Alaska and Canada are estimated for June–August 2004 assuming all wild fires were high-severity fires. (4) The $1 \times 1°$ species-specific emission estimates are determined using existing emission ratios from grassland, temperate and boreal eco-

systems from across North America [*Cofer et al.*, 1996a, 1996b; *Vose et al.*, 1996].

[13] Assuming high severity for all Alaskan and Yukon fires must be considered an upper bound on the actual emissions and results in the release of 70 Tg CO during the period from June–August 2004, which is a factor of 2 times higher the emissions obtained by *Pfister et al.* [2005] during the same period using MOPITT data to constrain inverse modeling based estimates of the Alaskan/Yukon emissions. In the future, improved emission estimates that account for changes in fire severity will be obtained using the U.S. Forest Service Haines Index. The Haines Index is the sum of a stability term and a moisture term. The sum provides an indication of the potential for the rate of spread (ROS) of a fire on a given day.

2.3. RAQMS Chemical Data Assimilation

[14] Data assimilation provides a statistically robust means of blending model predictions and observations to provide an optimal estimate of the true state of the atmosphere. Global assimilation of chemical measurements from polar orbiting satellites has been shown to improve estimates of the true atmospheric state [*Lamarque et al.*, 1999; *Jeuken et al.*, 1999; *Stajner et al.*, 2004] and is used by RAQMS to provide an optimal estimate of the global ozone distribution during INTEX-A. RAQMS uses the statistical digital filter (SDF) analysis system [*Stobie*, 1985, 2000] to perform a univariate assimilation of stratospheric profile and total column ozone observations. The SDF formalism is based on optimal interpolation (OI). However, rather than viewing the analysis as a minimization problem, SDF treats the analysis as a digital filtering problem [*Oppenheim and Schafer*, 1975]. In SDF, solving the OI equations at each grid point is equivalent to convolving a low-pass digital filter with the observation innovations (observed value minus first guess value). The spectral response of the filter is determined by the number of observations used per grid point, the observation spacing, the observation errors, the first guess and the first guess error correlation model [*Stobie*, 2000]. Estimates of the RAQMS forecast error variances are calculated by inflating the analysis errors (a by-product of the analysis) using the error growth model of *Savijarvi* [1995]. The quality control employed during the analysis includes a gross check, suspect identification and a buddy check for suspect observations.

[15] Stratospheric (tropopause and above) HALOE, SAGE II, and SAGE III solar occultation measurements were assimilated at 6 hour (0000 UT, 0600 UT, 1200 UT, 1800 UT) intervals to provide constraints on the stratospheric ozone mixing ratios. Solar occultation measurements occur during sunrise and sunset and are therefore limited to 14 observations spanning $360°$ of longitude within 2 narrow latitude bands per day. Assimilation of global TOMS V8 cloud cleared total column ozone measurements were used to provide constraints on the RAQMS total column analysis. The RAQMS column assimilation accounts for the vertical variation in the retrieval sensitivity by convolving the model first guess ozone profile with the zonal mean, time averaged sensitivity and the 3D monthly a priori used in the TOMS V8 retrieval algorithm. Special SAGE III limb scattering measurements [*Rault*, 2005; *Rault*
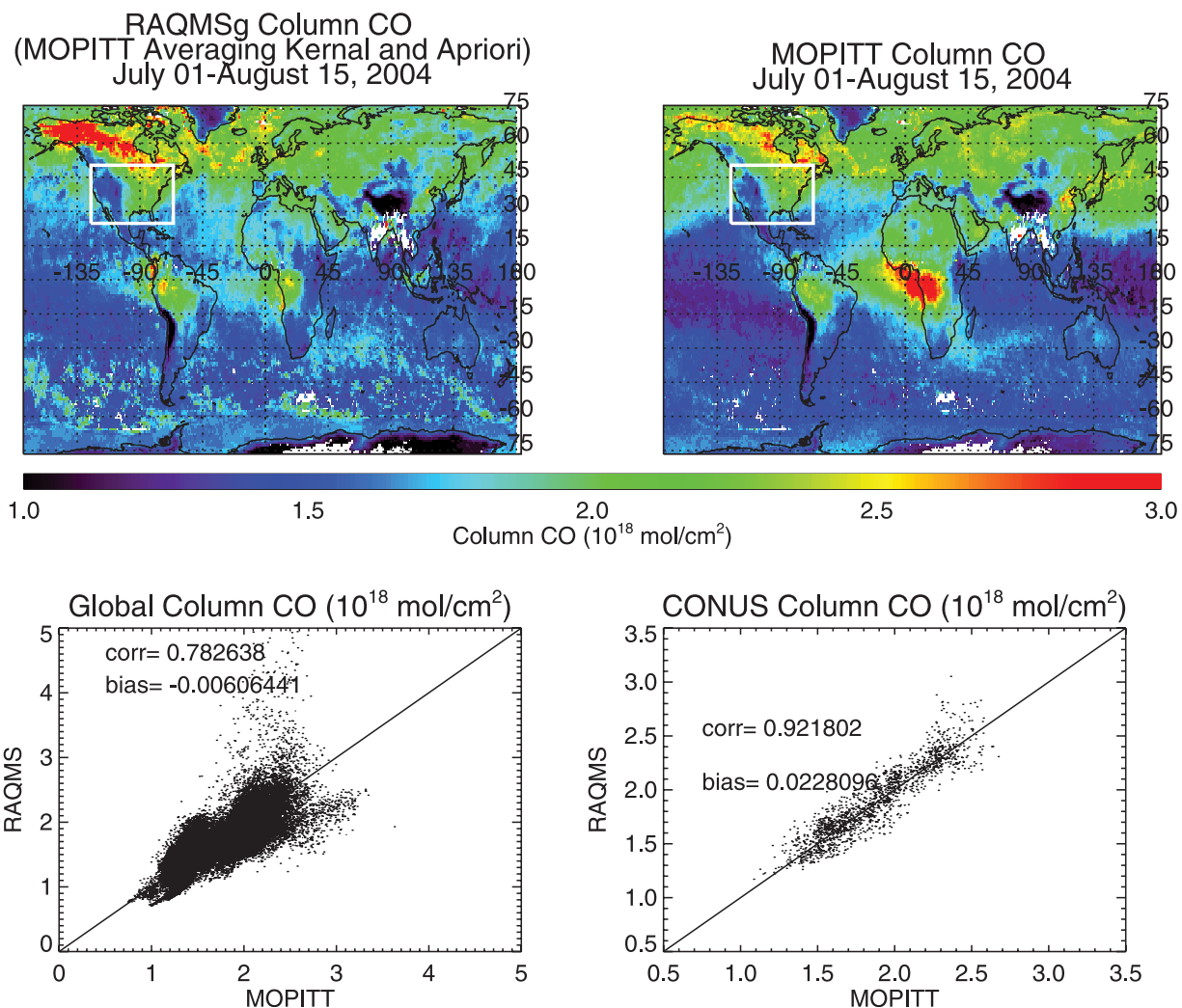
Figure 2. Comparison between RAQMS and cloud cleared MOPITT CO column (10^{18} mol/cm^2) for the period from 1 July to 15 August 2004. Continental U.S. budget domain is indicated in white.

and Taha, 2007] were taken on a daily basis over North America (24°N to 48°N, 150°W to 30°W) and the North Atlantic (40°N to 64°N, 30°W to 15°E) during the later half of July and mid-August. These measurements were also assimilated. Figure 1 shows a latitude time series of the location of observations used in the RAQMS assimilation. The symbols indicate the latitude and time periods when solar occultation and limb scattering observations were available while the contours indicate the density of the cloud-cleared total column measurements expressed as percentages of the total available observations at a given latitude. During Julian days 183–197 (1–14 July 2004) SAGE III and HALOE solar occultation measurements provide profile constraints in the Northern Hemisphere stratosphere. During Julian days 198–214 (15–31 July 2004) SAGE III limb scattering (restricted to North America and North Atlantic sectors) and SAGE II solar occultation measurements provide additional stratospheric constraints. During Julian days 215–226 (1–12 August 2004) there are very few stratospheric profile measurements to provide

constraints for the ozone assimilation in the Northern Hemisphere stratosphere.

3. Model Evaluation

3.1. Comparison With Satellite Observations

[16] Figure 2 shows the comparison between RAQMS and cloud cleared MOPITT CO column for the period from 1 July to 15 August 2004. The continental U.S. domain used in the budget calculations is also shown. To perform this comparison, 6 hourly RAQMS CO profiles were mapped onto MOPITT observation points and interpolated in time to the standard MOPITT retrieval levels, then the averaging kernel for each retrieval was used in conjunction with the MOPITT a priori to determine the "retrieved" RAQMS CO profile, which was integrated in the vertical using the MOPITT retrieval levels. The resulting RAQMS "retrieved" and MOPITT retrieved CO columns were binned in 1 × 1° bins. RAQMS is highly correlated with MOPITT on both regional (continental U.S. correlation is 0.902) and global (correlation is 0.708) scales. RAQMS
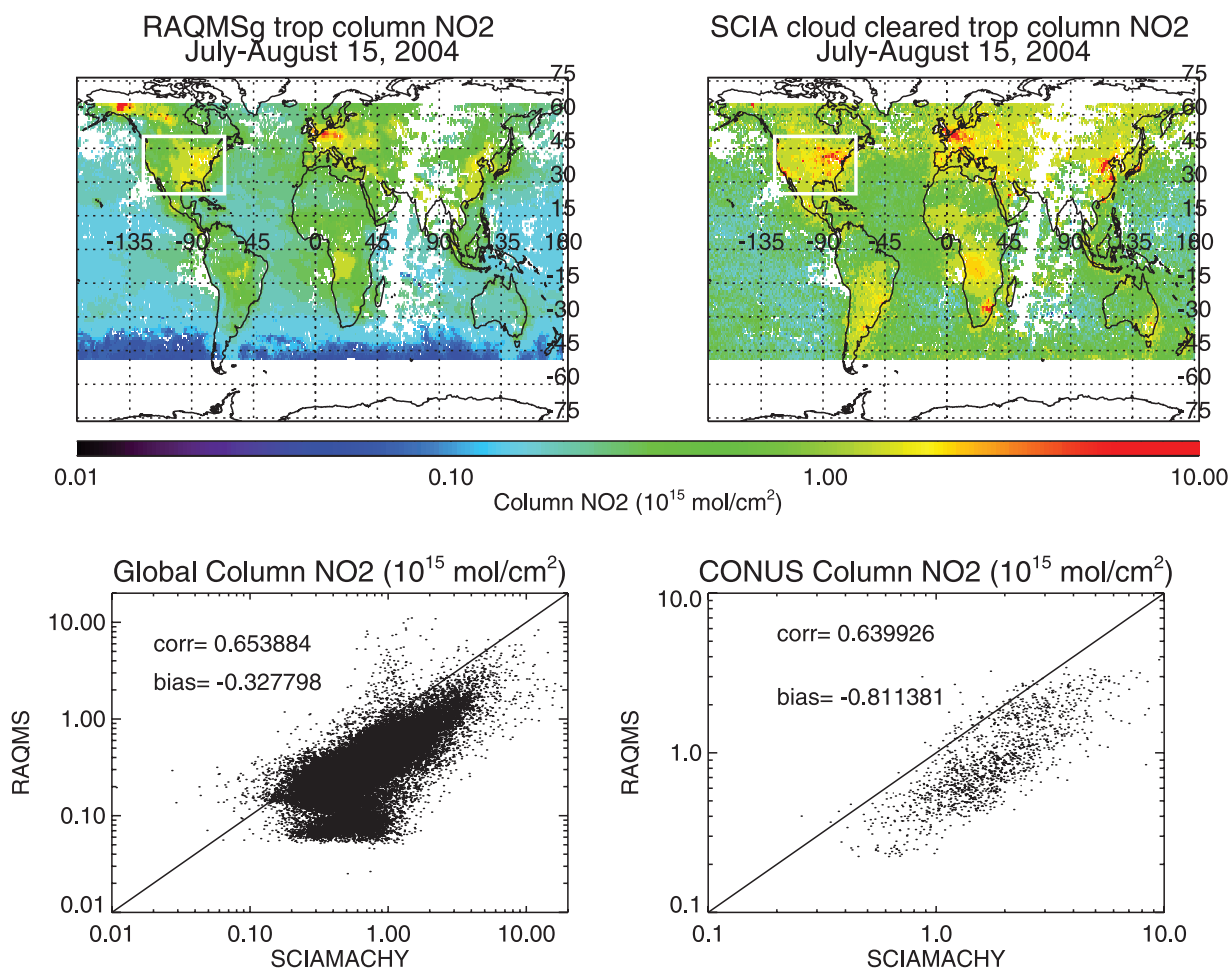
Figure 3. Comparison between RAQMS and cloud-cleared SCIAMACHY tropospheric NO2 column (10^{15} mol/cm^2) for the period from 1 July to 15 August 2004. Continental U.S. budget domain is indicated in white.

biases relative to MOPITT are very small (median biases of less than 0.01×10^{18} mol/cm^2, or <1%, globally and 0.02×10^{18} mol/cm^2, or 1.2%, over the continental United States). RAQMS overestimates the CO column relative to MOPITT over Alaska and western Canada, where the RAQMS "retrieved" column is up to a factor of 2 higher than MOPITT. This is consistent with the factor of 2 higher total wild fire emissions in the RAQMS simulation relative to the MOPITT constrained emissions used by *Pfister et al.* [2005]. RAQMS underestimates the CO column by 50% relative to MOPITT over central Africa. This is because climatological biomass burning emissions were used in this region. RAQMS also underestimates the CO column over S.E. Asia and the western Pacific.

[17] Figure 3 shows the comparison between RAQMS and cloud cleared tropospheric NO2 columns retrieved from SCIAMACHY by *Martin et al.* [2006] for the period from 1 July to 15 August 2004. The estimated uncertainty in the SCIAMACHY tropospheric NO2 columns is $\pm 5 \times 10^{14}$ mol/cm^2 +30% which includes systematic errors [*Martin et al.*, 2006]. In these comparisons, instantaneous RAQMS NO2 profiles were extracted from the model integrations at the SCIAMACHY observation points to account for the rapid diurnal variation in stratospheric NO2. We did not account

for the air mass factor used in the SCIAMACHY tropospheric NO2 retrieval when determining the RAQMS tropospheric NO2 column. However, we do not expect this omission to introduce significant biases in the comparison since the air mass factor calculation of the retrieval uses relative vertical NO2 profiles (shape factors) from GEOS-CHEM, which are largely determined by the spatial distribution of NOx emissions [*Martin et al.*, 2002], and are therefore similar between the two models. The resulting predicted and measured tropospheric NO2 columns were binned in $1 \times 1°$ bins. Because of the large dynamic range of the tropospheric column NO2 measurements the log of the NO2 columns are shown, however, the statistical analysis is based on the actual column amounts. As was found with MOPITT, the RAQMS spatial distribution is strongly correlated with SCIAMACHY (global correlation of 0.605 and continental correlation of 0.604) but RAQMS tends to underestimate tropospheric NO2 columns relative to SCIA-MACHY both globally (median bias of -0.33×10^{15} mol/cm^2, or 52% of the observed median NO2 column) and regionally (continental U.S. median bias of -0.81×10^{15} mol/cm^2, or 46% of the observed median NO2 column). Both of these biases are within the expected uncertainties in the SCIA-MACHY NO2 retrieval. The systematic low bias over most
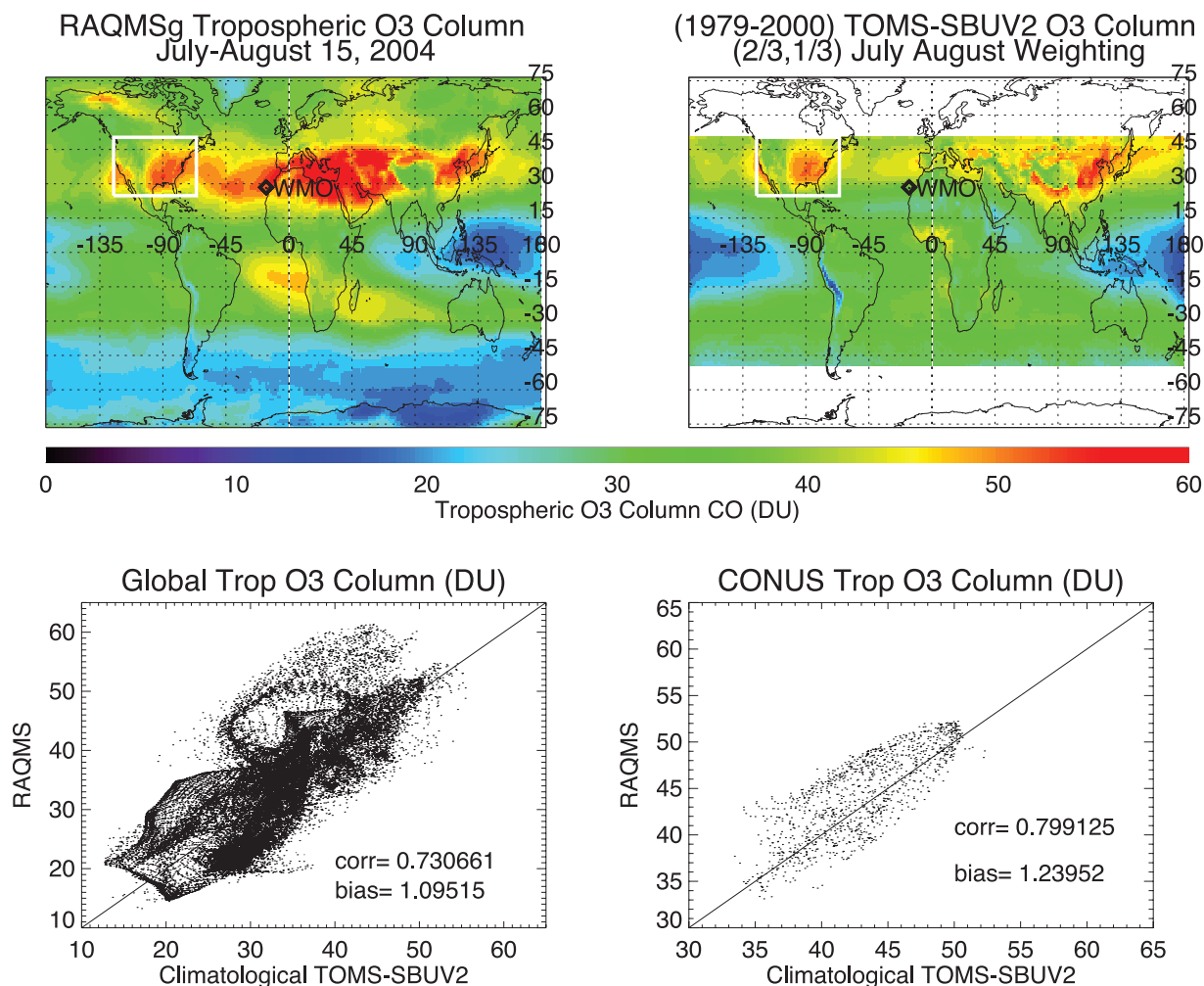
Figure 4. Comparison between RAQMS and climatological (1979–2000) tropospheric ozone column (DU) during the period from 1 July to 15 August 2004. Continental U.S. budget domain is indicated in white. The location of the WMO ozonesonde station at Santa Cruz, Tenerife, is indicated by a diamond.

of the Northern Hemisphere landmasses may be associated with underestimates in soil emissions [*Bertram et al.*, 2005; *Jaegle et al.*, 2005]. The relatively coarse resolution of the RAQMS simulation significantly impacts the inability to accurately describe urban "hot spots."

[18] Figure 4 shows the comparison between RAQMS and climatological (1979–2000) tropospheric ozone determined from TOMS total column and SBUV2 stratospheric measurements using residual techniques [*Fishman and Balok*, 1999]. To estimate the climatological 1 July to 15 August mean we have used a 2/3 to 1/3 weighting of the July and August climatological means. The RAQMS 2004 tropospheric ozone analysis is generally consistent with climatological expectations both globally (correlation of 0.703 and median bias of 1.09 DU, or 3%) and over the continental United States (correlation of 0.709 and median bias of 1.23 DU, or 3%) except over northern Africa and southern Europe, where the RAQMS analysis is approximately 10–20 DU higher than climatology. This broad region of elevated tropospheric ozone column is roughly coincident with the location of the subtropical jet and tropopause break, and was likely to be influenced

by stratosphere-troposphere exchange processes during INTEX-A.

[19] *Jing et al.* [2004], using contour advection of potential vorticity mapped SAGE II ozone measurements for 1990, showed enhanced (over 2 Tg/month) isentropic stratosphere to troposphere ozone transport along the 345 K potential temperature surface, which is roughly coincident with the midlatitude tropopause. The enhanced ozone transport extended in a broad meridional band from the N.E. United States, across the central Atlantic, and over northern Africa in a pattern that is remarkably similar to the Atlantic and European ozone enhancements found in the RAQMS ozone analysis. There is some evidence of this pattern in the TOMS-SBUV2 climatology, however, the *Fishman and Balok* [1999] TOMS-SBUV2 climatology only includes tropospheric ozone residuals that are less than 75 DU, which would tend to filter out influences of stratosphere to troposphere exchange processes on the climatological tropospheric ozone.

[20] To determine whether this column ozone enhancement is real or a model artifact we compared the RAQMS ozone analysis to eight World Meteorological Organization
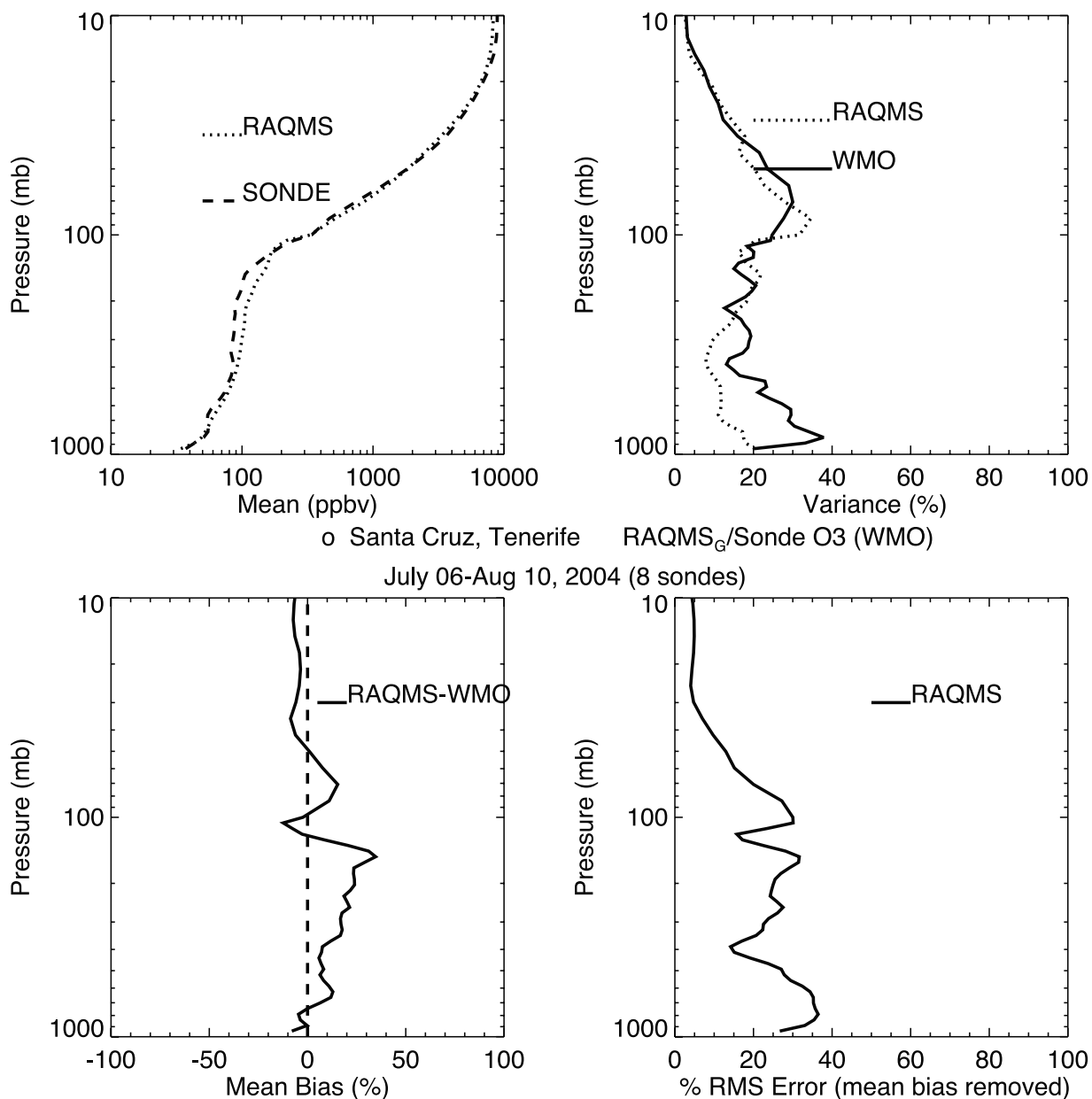
Figure 5. Comparison between RAQMS and Santa Cruz, Tenerife, ozonesondes during 6 July to 10 August 2004.

(WMO) ozonesondes that were launched during the period from 8 July to 10 August 2004 from Santa Cruz, Tenerife (location shown on Figure 4). Figure 5 shows results from the statistical analysis of the WMO ozonesonde data. The observed ozone profile shows persistent ozone enhancements (mean values of 80 ppbv) above 500 mbar. Compared to the WMO ozonesonde data, the Santa Cruz RAQMS ozone analyses shows mean high biases of 10% or less below 400 mbar. However, the high bias in the RAQMS analysis increases to nearly 35% at the tropopause (near 150 mbar), suggesting that while there is clearly upper tropospheric ozone enhancement at Santa Cruz it is overestimated in the RAQMS ozone analysis. A 35% overestimate in upper tropospheric ozone has a relatively small effect on the tropospheric ozone column. The mean observed and analyzed ozone columns below 150 mbar were

43.9 DU and 48.4 DU, respectively. The resulting 4.5 DU overestimate is approximately 10% of the observed column.

3.2. Comparison With IONS Ozonesonde and EPA AIRNOW Networks

[21] The INTEX Ozonesonde Network Study (IONS) [*Thompson et al.*, 2007b] provided multiple daily ozonesonde launches throughout the continental United States and southern Canada during INTEX-A. The unprecedented duration (1 July to 14 August), frequency (daily), and density (up to 12 ozonesonde stations) makes this data set extremely useful for verification of the RAQMS ozone assimilation as well as science studies [*Thompson et al.*, 2007a]. Figure 6 shows composite time series of the IONS ozonesonde data along with comparisons with the RAQMS ozone analysis. The IONS composite was obtained by
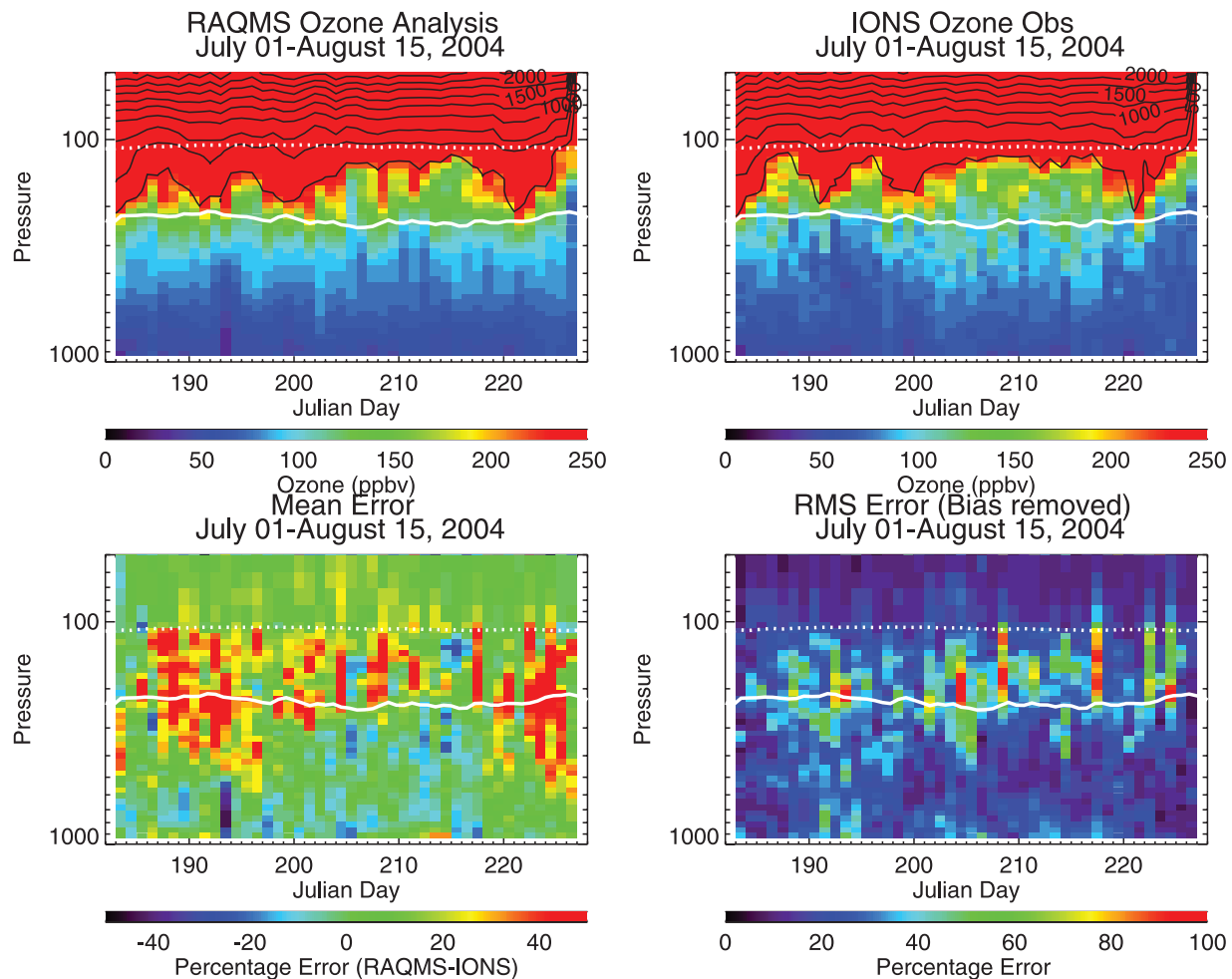
Figure 6. (top) Composite time series of IONS ozonesonde data and coincident RAQMS ozone analyses (ppbv) during the period from 1 July to 15 August 2004. (bottom) Composites of mean and RMS (mean bias removed) errors (%).

binning all the daily ozonesondes in log-pressure bins (10 bins/decade in pressure). The RAQMS composite was obtained in the same manner after mapping the RAQMS ozone analysis to the full resolution ozonesonde. Mean errors were estimated by averaging the point-by-point errors for all profiles within each pressure bin. RMS errors were estimated in the same way after removing the mean bias within each pressure level. The daily mean pressure of the thermal tropopause on the northern boundary of the continental U.S. budget domain, and 380 K potential temperature surface on the southern boundary of the budget domain are also indicated. These surfaces define the maximum vertical extent of the middle world [*Holton et al.*, 1995] over the continental United States. The middle world is a region in the lower stratosphere that is strongly coupled to the subtropical upper troposphere because of quasi-horizontal, isentropic exchange near the subtropical jet. This quasi-horizontal exchange occurs because of the sharp meridonal gradient in the tropopause altitude near the subtropical jet. The IONS composite shows significant day to day variability in this region, as evidenced by the altitude of the 250 ppbv ozone mixing ratio (which is roughly coincident

with the thermal tropopause) prior to mid-July (Julian day 200) then there is an extended period with less variability, followed by renewed variability during early August (Julian day 215). The RAQMS ozone analysis does a good job in reproducing this composite behavior, which is largely driven by upper tropospheric planetary wave activity.

[22] Upper tropospheric ozone mixing ratios of 100 ppbv or more are most likely stratospherically influenced air masses. The IONS composite shows significant variability in the frequency of stratospherically influenced tropospheric ozone measurements, defined here as composite ozone mixing ratios greater than 100 ppbv but observed below northern tropopause of the continental U.S. domain. In the IONS composite, signatures of stratospherically influenced ozone extend down to 500 mbar during the middle 3 weeks of INTEX-A. There are relatively fewer observations of stratospheric influenced air in the troposphere during the first 2 weeks of July (Julian days 183–198) and second week of August (Julian days 227–234). This is consistent with *Fairlie et al.* [2007] who find evidence for interleaving and mixing of stratospherically influenced and polluted
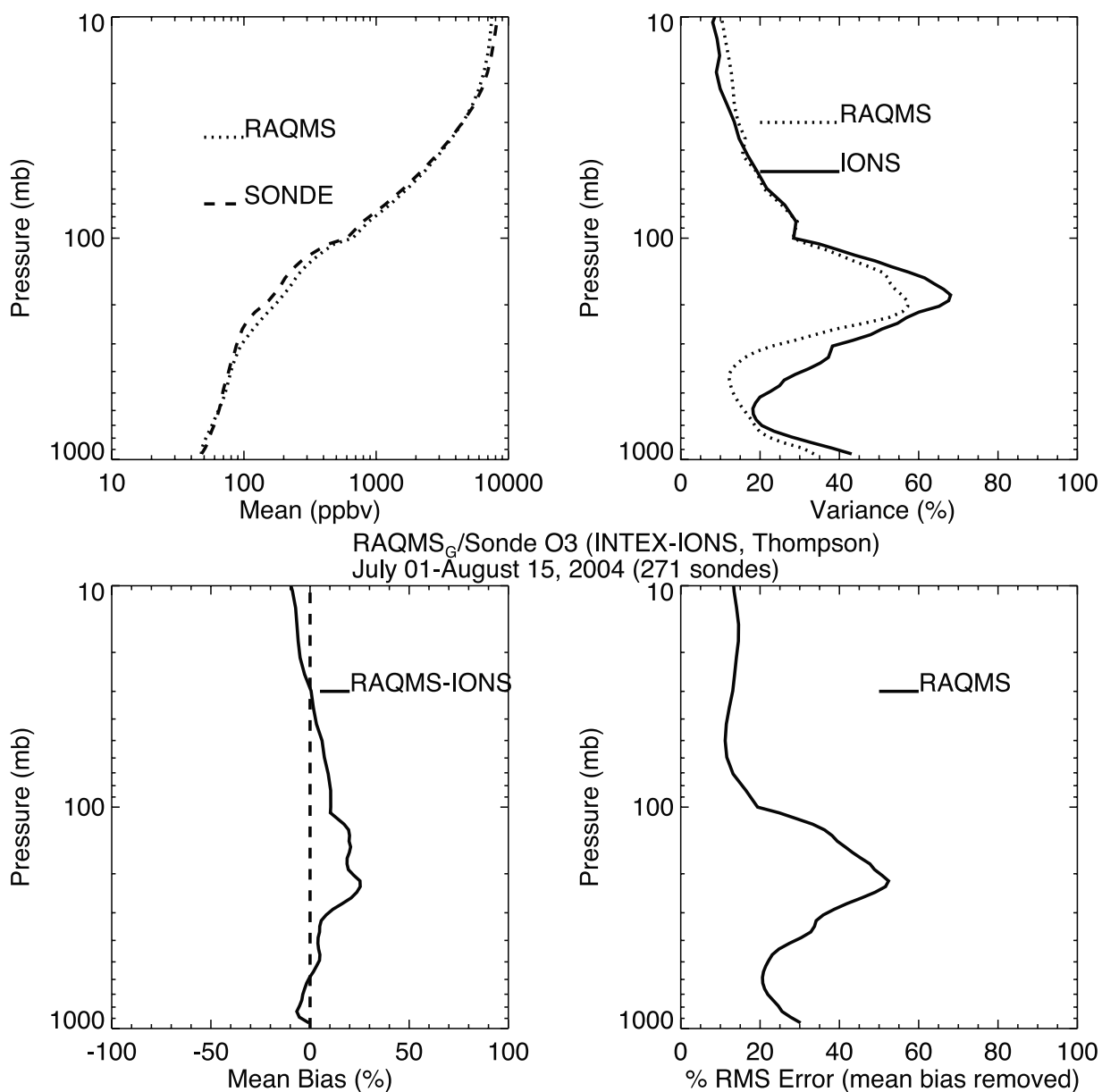
Figure 7. Comparison of time averaged IONS ozonesonde and coincident RAQMS ozone analyses during 1 July to 15 August 2004.

tropospheric air in the vicinity of the subtropical jet for INTEX-A flights in late July and early August.

[23] The observed variations in the depth of the stratospherically influenced air in the upper troposphere are not as pronounced in the RAQMS composite, leading to predominately positive analysis errors in the upper troposphere during the beginning and end of INTEX-A and predominately negative analysis errors in the upper troposphere during the middle of INTEX-A. The positive analysis errors at the beginning an end of the mission frequently reach 40–50% and extend down to as far as 600 mbar while the negative analysis errors are typically only 20–30%. During the last two weeks of July and first week of August the frequency and vertical extent of large positive analysis errors are significantly reduced, with the majority of the

analysis errors between ±20% during the middle part of INTEX-A.

[24] The first part of this period of relatively low analysis errors (15–31 July) corresponds to the period when daily SAGE III limb scattering measurements, made over a wide latitude band over the continental United States, were assimilated. The reduction in the extent and frequency of significant high biases in the analysis during this period indicates that the assimilation of SAGE III limb scattering measurements had a positive impact on the RAQMS ozone analysis, particularly in the upper troposphere/lower stratosphere. The fact that these improvements persist for at least 5 days after the limb scattering assimilation stops indicates that the system has memory of the measurements, which has significant implications for air quality forecasting. The RMS analysis errors over the continental United States are
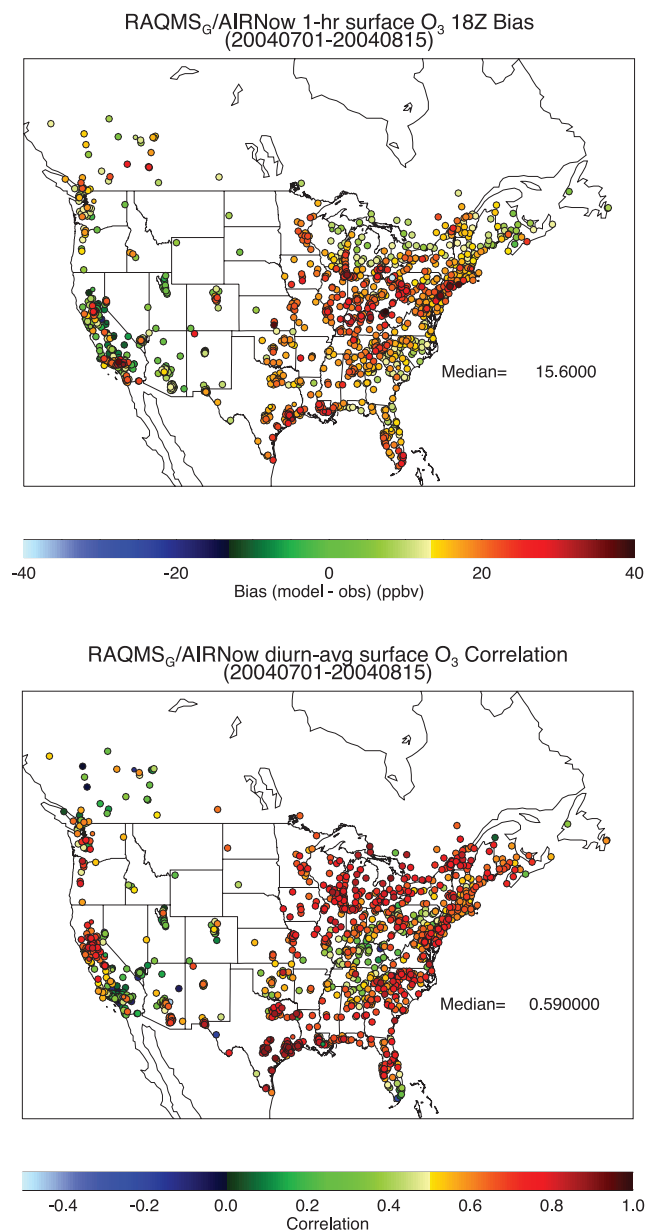
RAQMS$_G$/AIRNow 1-hr surface O$_3$ 18Z Bias
(20040701-20040815)

Median=   15.6000

Bias (model - obs) (ppbv)

RAQMS$_G$/AIRNow diurn-avg surface O$_3$ Correlation
(20040701-20040815)

Median=   0.590000

Correlation

Figure 8. Comparisons between RAQMS and EPA AIR-NOW surface ozone measurements during 1 July to 15 August 2004.

largest within the middle world and are typically on the order of 40–60%, although occasionally RMS errors reach up to 80–100%. These errors are most likely associated with errors in the vertical placement of stratospheric and subtropical ozone lamina that were frequently observed during INTEX-B [*Thompson et al.*, 2007a]. There are occasional RMS errors of up to 40% near the surface, but these appear to occur during periods of relatively low boundary layer ozone events and are not likely to be significant.

[25] Figure 7 summarizes the RAQMS/IONS comparison with a time averaged comparison between the RAQMS ozone analysis and all ozone profiles during INTEX-A. In addition to mean and RMS errors we also assess the ability of the RAQMS analysis to capture the observed variability,

defined here as the overall temporal and site to site variability at a given pressure level. Above 100 mbar, the mean analysis biases are on the order of 10% with RMS errors of less than 20%. The upper troposphere/lower stratosphere shows mean high biases of near 20%, extending from 100 to 300 mbar, below 300 mbar, the RAQMS shows low biases of less than 10%. The RAQMS analysis captures the majority of the observed variance enhancement in the lower stratosphere and continental boundary layer but also shows large RMS errors (near 50% at 200 mbar). These RMS errors are due to vertical displacement of filaments of high and low ozone associated with stratosphere-troposphere exchange processes.

[26] Figure 8 shows comparisons between RAQMS surface ozone and ozone measurements from the EPA AIR-NOW network [*Wayland et al.*, 2002]. These maps show mean statistics based on time series analysis for the individual AIRNOW stations. The median temporal correlation between the 6 hourly RAQMS prediction and coincident 1 hour AIRNOW measurements is 0.702 (not shown), and largely reflects the diurnal cycle in surface ozone. To assess the ability of the RAQMS ozone analysis to capture daily variations in surface ozone we consider correlations between the diurnally averaged RAQMS analysis and coincident AIRNOW measurements. The median correlation between diurnally averaged RAQMS and AIRNOW data is 0.590 with lowest correlations in the diurnally averaged ozone found over West Virginia, southern California, and the western mountain states.

[27] To assess the ability of the RAQMS ozone analysis to capture daytime photochemistry we compiled station-by-station mean biases at 1800 UT, which is midday over much of the central and eastern United States. The 1800 UT mean biases are generally positive with a median value of 15.6 ppbv. The 1800 UT mean biases are largest within the Mississippi and Ohio River valleys. The daytime mean biases may be associated with overestimates in surface ozone production, overestimates in boundary layer O3 entrainment, assimilation of TOMS column ozone (which occurs during the 1800 UT assimilation cycle over North America), or overestimates in the initial (morning) surface ozone. Overestimates in surface ozone production would suggest excess NOx, however column NO2 is actually underestimated (particularly in urban areas) on the basis of the RAQMS/SCIAMACHY comparison. Entrainment is also unlikely to account for the 1800 UT bias since boundary layer O3 is actually underestimated (in the mean) on the basis of the RAQMS/IONS comparison. This leaves overestimates in the initial (morning) surface ozone or TOMS column ozone assimilation as the most likely reasons for the mean daytime bias. Nighttime (0000 UT) biases show a similar pattern with median values of 18.1 ppbv. The 0000 UT biases are frequently associated with underestimates in nighttime titration of ozone, which is a near-surface phenomena that is not accurately captured within RAQMS. *McKeen et al.* [2005] compared the real-time air quality forecast skill for 7 regional models during the 2004 ICARTT field mission. The regional model domains generally included the NE and SE United States at resolutions ranging from 12 km to 42 km. Correlation coefficients between the forecasted and observed 8 hour averaged ozone ranged from 0.55 to 0.75, with 8 hour averaged high ozone
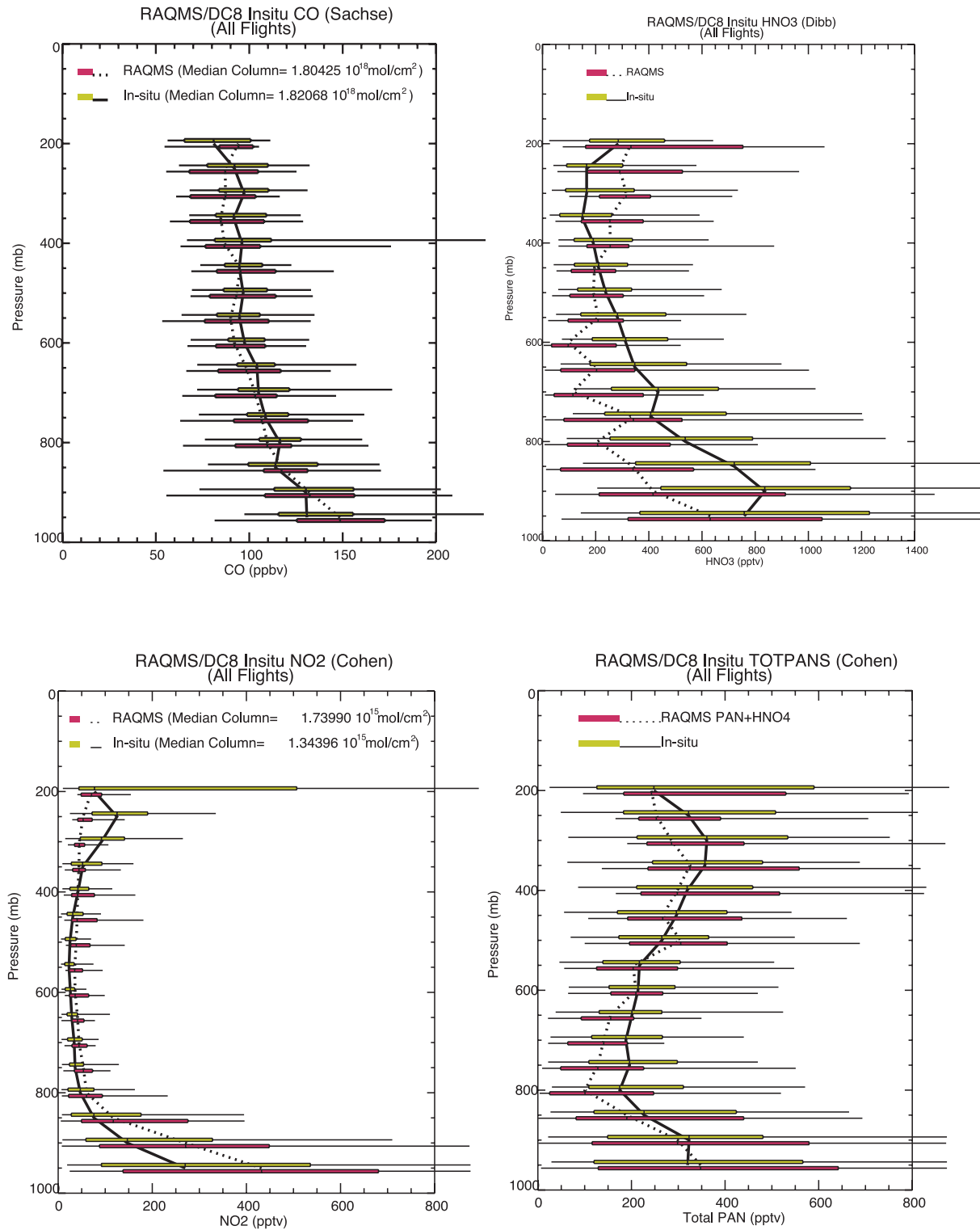
Figure 9a. Comparisons between RAQMS and INTEX-A DC8 in situ observations of (top left) CO, (top right) HNO3, (bottom left) NO2, and (bottom right) total PANs during 1 July to 15 August 2004. CO is in ppbv, and NO2, total PANs, and HNO3 are in pptv.

bias ranging from 3 to 27 ppbv. While the RAQMS diurnally averaged correlations and 1800 UT biases are not directly comparable to the regional model statistics the RAQMS/AIRNOW comparisons are generally consistent with the results of comparisons between AIRNOW and higher-resolution regional air quality forecast models during ICARTT.

3.3. Comparison With DC8 in Situ Measurements

[28] Figure 9 shows comparisons with in situ CO, O3, NO2, total PAN (TPAN), and HNO3 data obtained by
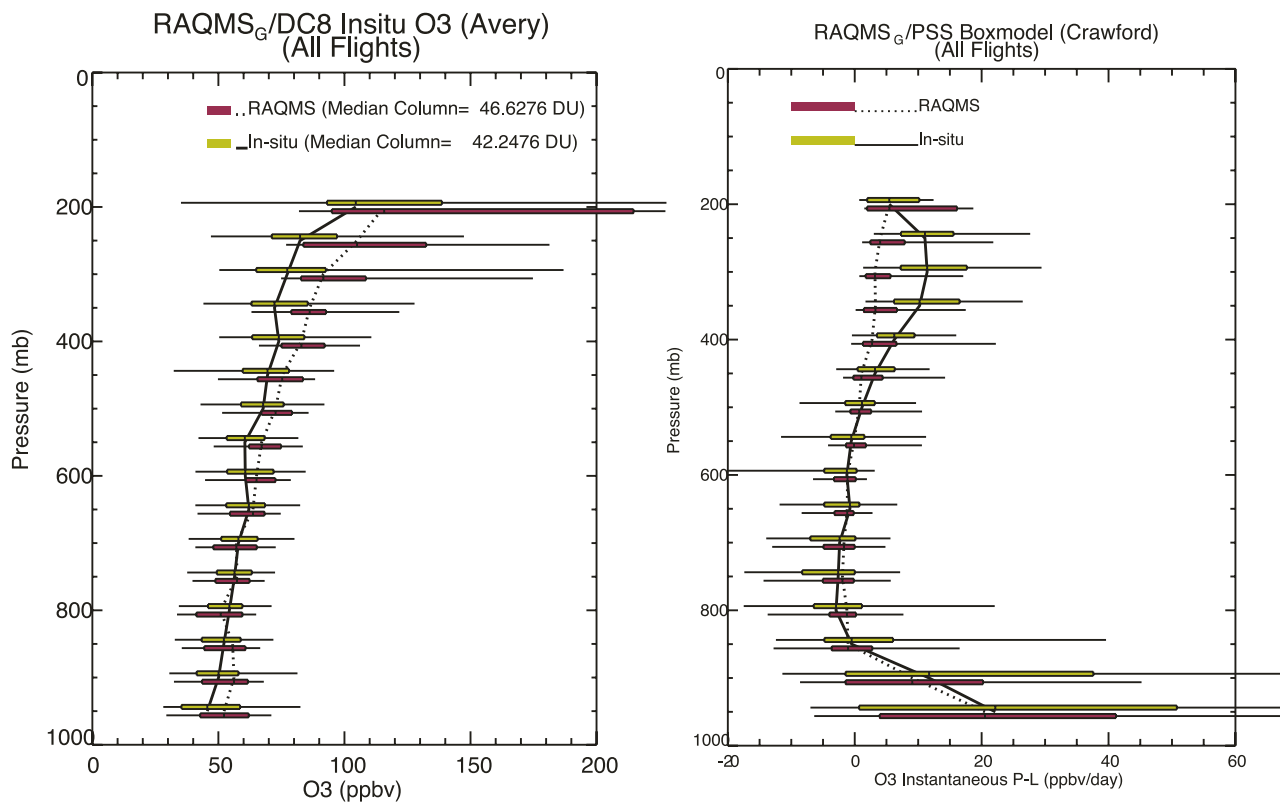
Figure 9b. (left) Comparisons between RAQMS and INTEX-A DC8 in situ observations of O3 and (right) observationally constrained box model P-L calculations during 1 July to 15 August 2004. O3 is in ppbv, and P-L is in ppbv/day.

instruments on board the NASA DC8 during all flights during INTEX-A as well as observationally constrained photochemical steady state calculations from the LaRC box model [*Olson et al.*, 2006]. These comparisons were made by interpolating the RAQMS chemical fields onto the DC8 flight track and sampling the model at the frequency of the in situ measurements, then binning the modeled and measured values into 50 mbar pressure bins. The median (vertical profile), 50th (bar) and 90th (whisker) percentiles of the modeled and observed distributions within each pressure bin are shown. The modeled CO is 5–10 ppbv lower than observed except at 950 mbar where the model is approximately 20 ppbv higher than in situ measurements. Predicted and observed column amounts, obtained by integrating the median number densities between 1000 and 250 mbar, are 1.8×10^{18} and 1.82×10^{18} mol/cm^2, respectively. The 1–2% agreement between the predicted and in situ median column amounts is consistent with the comparison between the RAQMS and MOPITT CO columns, which showed median biases of 1.2% over the continental United States. RAQMS background CO mixing ratios are generally low relative to airborne in situ data [*Kiley et al.*, 2003]. The good agreement in RAQMS CO relative to in situ and MOPITT measurements over continental United States and the high bias in RAQMS CO relative to MOPITT measurements over Alaska and Canada during 2004 suggests that overestimates in wild fire emissions are compensating for underestimates in background CO concentrations over the continental United States in the

RAQMS INTEX-A simulations. *Warneke et al.* [2006] show that as much as 30% of the CO enhancement observed over the NE United States is attributable to the Alaskan and Canadian wild fires.

[29] The modeled O3 is within 10 ppbv below 400 mbar and approximately 20 ppbv higher than the observations above 400 mbar. The 10 ppbv overestimate of the median ozone mixing ratios below 900 mbar accounts for about 65% of the median biases in surface ozone found in the AIRNow analysis. Since the DC8 primarily sampled continental background conditions over the southeastern United States this indicates that a significant part of the high biases at the surface is due to overestimates in background ozone mixing ratios over the depth of the boundary layer. The column densities obtained from integration of the median analyzed and in situ ozone profiles are 46.6 and 42.2 DU, respectively, resulting in a 10% error in the median ozone column relative to the aircraft measurements. The 20–25% differences between the RAQMS ozone analysis and in situ mixing ratios in the upper troposphere are consistent with the comparison between RAQMS and the IONS ozone-sonde data, suggesting that the analyzed tropospheric O3 column is within 10% of the actual column over the continental United States. The modeled NO2 is approximately 50 ppbv low (factor of 2) relative to the measurements at 300 mbar and larger than observed below 800 mbar. The predicted median NO2 mixing ratio is a factor of 2 larger than observed at 950 mbar. Column NO2 densities, based on integration of the predicted and observed median

profiles, are 1.74×10^{15} and 1.34×10^{15} mol/cm^2, respectively, resulting in a 30% high bias in the median NO2 column relative to the aircraft measurements. This high bias in median NO2 column density is not consistent with the 46% negative median bias found relative to SCIAMACHY tropospheric NO2 column densities. The differences between the results of the SCIAMACHY and in situ model evaluation studies could arise from low biases in the RAQMS NO2 mixing ratios below the 1000 ft minimum altitude of the DC8 or biases in the SCIA-MACHY retrieval. Total PANs (peroxynitrates) are within 50 pptv of the observed mixing ratios except for near 800 mbar where the modeled total PAN (PAN+HNO4) is low by 75 pptv. HNO3 is low by 200–400 pptv below 600 mbar and high by 150 pptv at 300 mbar. The modeled ozone P-L is in very good agreement with observationally constrained photochemical steady state calculations except at 300 mbar where the modeled P-L (1 ppbv/day) is low by a factor of 2. This underestimate in ozone P-L is consistent with factor of 2 underestimate of NO2 at this altitude. The fact that the model ozone overestimates are associated with overestimates in HNO3 and underestimates in P-L, NO2 and TOTPANS, suggests that the model overestimates strato-spheric influences (high O3, HNO3), underestimates con-vective influences (P-L, NO2, PAN), or both in the upper troposphere.

3.4. Comparison With P3 in Situ Measurements

[30] During ICARTT, NOAA conducted the New England Air Quality Study-Intercontinental Transport and Chemical Transformation (NEAQS-ITCT) mission during which the P3 aircraft conducted flights in the NE United States which sampled primary anthropogenic emission sources and subsequent transport and chemical transforma-tion within the NE United States [*Fehsenfeld et al.*, 2006]. The P3 flights provide extensive measurements within the urban boundary layer and provide additional insight into how the model represents O3 and NOy in the highly populated NE United States. Figure 10 shows comparisons with in situ O3, NO2, and Sum NOy data obtained by instruments on board the NOAA P3 during all flights during ICARTT. A map of all of the P3 flights is also shown. The modeled NOy is systematically lower than the P3 measure-ments by 30–40% below 700 mbar. This low bias is primarily due to underestimates in HNO3 (not shown), consistent with the low bias with the DC8 HNO3 measure-ments shown in Figure 9. The modeled NO2 is in very good agreement with the P3 measurements except at 950 mbar where the model has a 30% high bias. The predicted median NO2 column, obtained by integrating the median number densities between 1050 and 500 mbar, is within 2% of the column obtained from the P3 measurements. The RAQMS ozone analysis is generally within 5 ppbv of the P3 measurements. In contrast to the DC8 O3 comparison, the median ozone mixing ratios are in very good agreement with the P3 measurements below 900 mbar. The P3 pri-marily sampled urban outflow conditions in the northeastern United States, which is a region where the RAQMS surface ozone biases with respect to AIRNOW where quite large. This indicates that the surface biases within the northeastern United States are relatively shallow, and suggests that underestimates in nighttime NOx titration play a significant

role in the daytime biases found relative to AIRNOW in urban regions. Integration of the analyzed and observed median O3 number densities results in column ozone abundances that are within 1–2% over the NE United States.

4. Global and Continental U.S. Estimates of Ozone and NOy STE

[31] The preceding discussion highlights the important role that stratospheric-tropospheric exchange (STE) plays in determining the distribution of ozone and NOy (primarily HNO3) in the upper troposphere during INTEX-A. In this section, we follow the discrete approach outlined by *Pierce et al.* [2003] to estimate the contribution of STE to the global distribution of upper tropospheric ozone during INTEX-A. In the work by *Pierce et al.* [2003] the regional component of RAQMS was used to determine discrete, cross-tropopause ozone fluxes over S.E. Asia during the NASA TRACE-P mission. The discrete cross tropopause flux was estimated by computing instantaneous horizontal and vertical fluxes out of tropospheric grid boxes that were adjacent to the model tropopause, using the WMO thermal tropopause definition. Here we apply the same approach using the global component (UW-Hybrid dynamical core) of RAQMS. The UW-Hybrid model is formulated in hybrid isentropic-eta coordinates and consequently grid boxes are defined in the vertical by potential temperature surfaces above 345 K, or roughly the midlatitude tropopause. This hybrid isentropic-eta formulation of the UW-Hybrid dynam-ical core allows us to explicitly compute the isentropic (quasi-horizontal) exchange of stratospheric and tropo-spheric air across the tropopause break, which extends from roughly 345 K to 380 K in potential temperature. This region of the lower stratosphere, bounded by the tropopause and the 380 K potential temperature surface, is coupled to the upper tropical troposphere through isentropic exchange of mass, momentum, and trace gases.

[32] Figure 11 shows the zonally averaged cross tropo-pause ozone and NOy fluxes during the period from 1 July to 15 August 2004. The ozone and NOy fluxes across the 380 K potential temperature are also shown. NOy fluxes are determined by computing the instantaneous 6 hourly fluxes of individual components of NOy and then adding them together. The RAQMS first guess odd oxygen (Ox) is used to compute the 6 hourly ozone fluxes to assure dynamical consistency between the Ox and forecasted winds. The time averaged cross tropopause ozone and NOy flux is deter-mined by averaging 6 hourly calculations of horizontal (isentropic) and vertical (diabatic) fluxes, and movement (in altitude) of the tropopause. Since the 380 K surface is a model level, the horizontal velocities at 380 K are parallel to the 380 K surface and the time averaged ozone and NOy flux at 380 K only includes vertical fluxes plus movement (in altitude) of the 380 K surface.

[33] In the tropics, the ozone and NOy fluxes are upward (positive) with net transport through the tropopause and 380 K potential temperature surface into the lower strato-sphere. This transport is driven by radiative heating and upward diabatic vertical motion. In polar regions, the diabatic transport of ozone and NOy across the 380 K potential temperature surface is downward and driven by
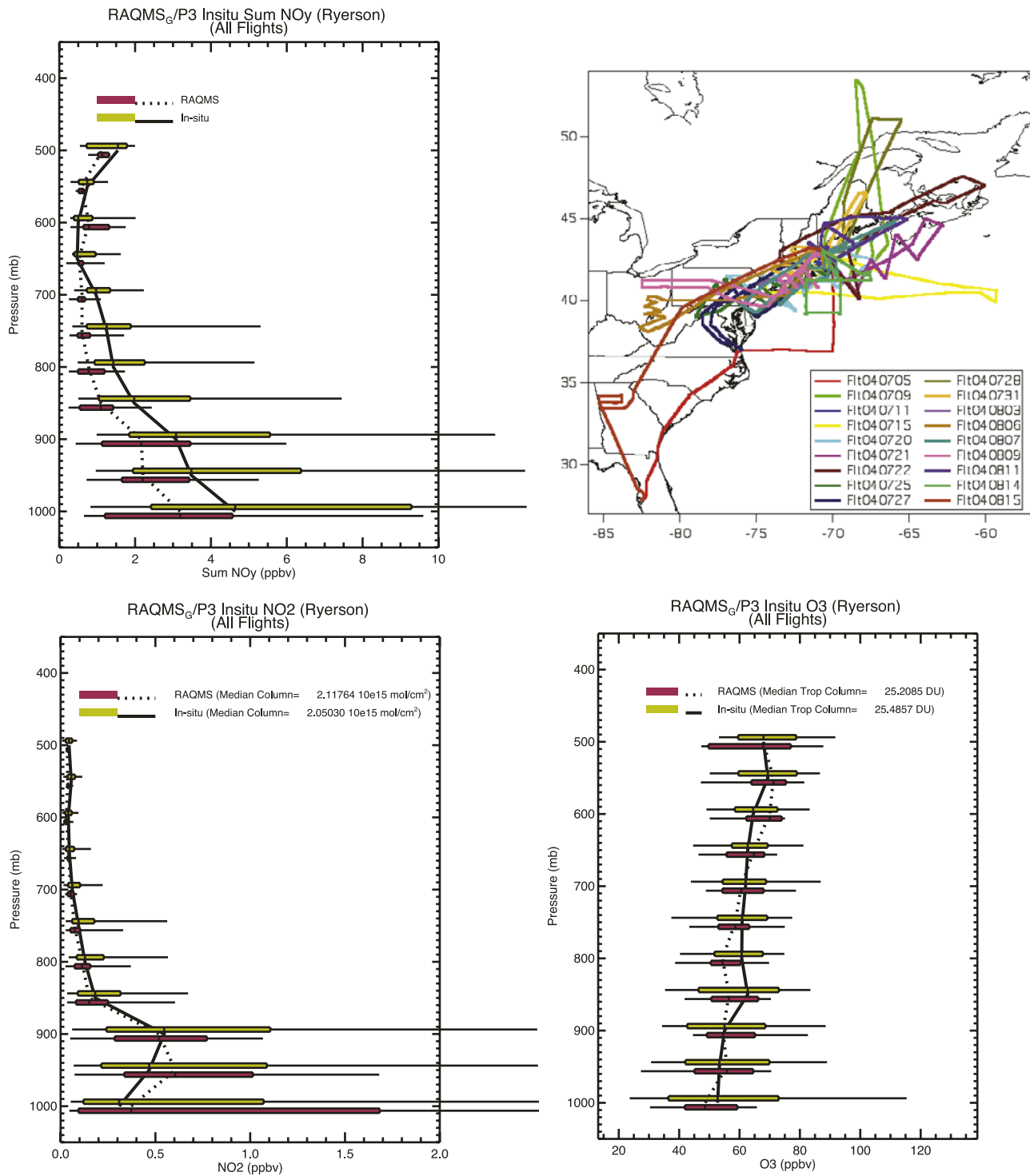
Figure 10. Comparisons between RAQMS and ICARTT P3 in situ observations of (top left) sum NOy, (top right) NOAA P3 flight tracks, (bottom left) NO2, and (bottom right) O3 all in ppbv, during 1 July to 15 August 2004. P3 data are provided by Thomas Ryerson, NOAA Aeronomy Laboratory.

radiative cooling. The net transport of ozone and NOy across the polar tropopause is also downward, but it occurs through the combined effects of downward diabatic motion and secular changes (increases) in the altitude of the polar tropopause, which compensate for net horizontal (isentropic) fluxes of ozone and NOy into the middle world. At the

tropopause break, horizontal (isentropic) ozone and NOy fluxes from the troposphere into the stratosphere dominate.

[34]   These results are consistent with mass flux estimates by *Schoeberl* [2004] who used explicit calculations of the diabatic fluxes through the 380 K potential temperature surface and tropopause, along with mass tendencies within
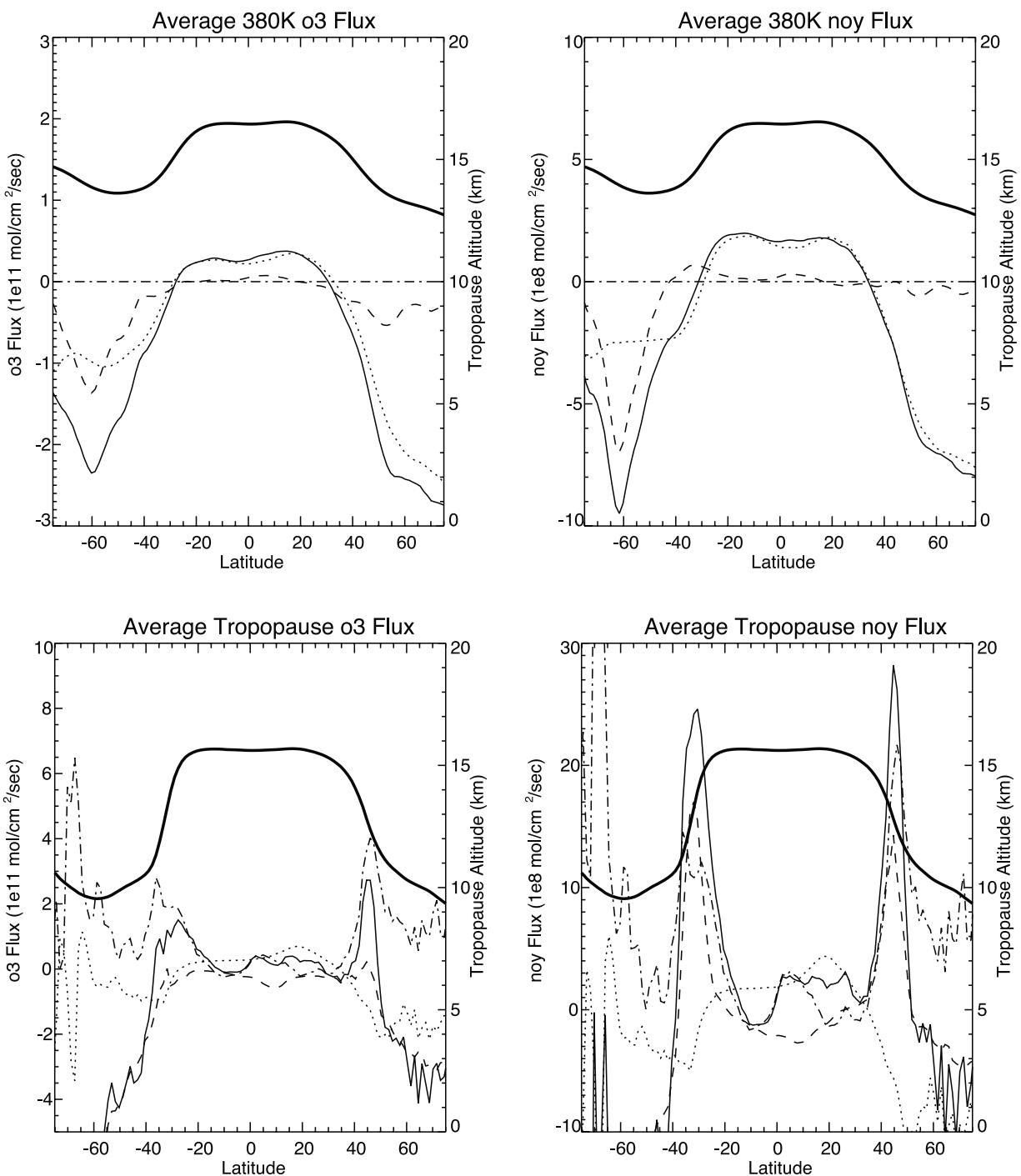
Figure 11. Zonally averaged global (top) 380 K and (bottom) cross tropopause fluxes of (left) O3 (10^{11} mol/cm^2/s) and (right) NOy (10^8 mol/cm^2/s) during 1 July to 15 August 2004. The thin solid line is the net flux, which is the sum of isentropic (dash-dot), diabatic (dotted), and movement of the surface (dashed). The bold line denotes the mean altitude (km) of the 380 K and tropopause surface.

the middle world, to estimate adiabatic (isentropic) exchange through the tropopause. He found net adiabatic fluxes across the tropopause were positive (into the middle world) throughout the year. However, because the adiabatic term was obtained as a residual, he was not able to determine the latitudinal distribution of the adiabatic cross tropopause flux. The RAQMS analysis shows that the adiabatic flux is largest at the tropopause break. This net flux (from above and below) of trace gases into the middle world on the poleward side of the tropopause break introduces the possibility for accumulation of ozone and NOy

with both stratospheric and tropospheric origins within this region.

[35] Figure 12 shows the zonally averaged cross tropopause ozone and NOy fluxes during the period from 1 July to 15 August 2004 for the continental U.S. budget domain. The regional ozone and NOy fluxes across the 380 K potential temperature surface are also shown. The cross tropopause fluxes of ozone and NOy over the continental United States are dominated by quasi-horizontal (isentropic) transport into the middle world. The both ozone and NOy show peak troposphere to stratosphere ozone fluxes at 45°N with the cross tropopause NOy flux being dominated by transport of HNO3. The fluxes of ozone and NOy across the 380 K potential temperature surface are largest on the northern boundary of the budget domain and are dominated by downward (diabatic) transport into the middle world. These results are consistent with the global flux estimates for this latitude band and suggest that there should be an accumulation of ozone and NOy, some of tropospheric and some of stratospheric origin, in the lower stratosphere over the continental United States during INTEX-A. The net upward flux of ozone and NOy at the tropopause within the continental U.S. budget domain suggests that the strato-spherically influenced tropospheric air observed in the IONS composite must have entered the troposphere pole-ward of the continental U.S. domain, where net cross tropopause fluxes are downward.

5. Ozone and NOy Budgets Over the Continental United States

5.1. Ozone Budget Analysis

[36] Ozone assimilation reduces errors in the budget analysis by providing an improved estimate of ozone within the continental U.S. budget volume. However, assimilation introduces nonphysical changes in ozone that must be isolated from the physical and chemical processes accounted for in the RAQMS simulation. To isolate the influences of assimilation in the budget calculations we use the RAQMS first guess ozone distributions to compute the lateral and diabatic fluxes. Since the first guess ozone has been advected for the previous 6 hours with forecasted wind fields and experienced the effects of the predicted photo-chemistry, the first guess is dynamically and chemically consistent. The ozone analysis increment is treated as a separate (although nonphysical) budget term. This approach allows us to isolate the effects of assimilation in the budget calculations.

[37] Figure 13 shows the time averaged zonal mean distribution of continental U.S. ozone, net P-L, convective mixing tendencies, and the mean absolute value of the assimilation increment. The mean location of the middle world, bounded by the thermal tropopause and 380 K potential temperature surface, is also indicated. Mean ozone mixing ratios are above 80 ppbv in the northern upper troposphere and range from 200 to 350 in the middle world. Lower tropospheric ozone mixing ratios are less than 55 ppbv, with no clear indication of a surface enhancement. Time averaged upper tropospheric net ozone production (P-L) reaches 4.0 ppbv/day at 10 km and 30N, and shows net photochemical destruction below 7 km in the southern portion of the domain. Net photochemical production

reaches 10 ppbv/day in the continental U.S. boundary layer. Deep convection in the southern part of the domain leads to upper level detrainment of low ozone mixing ratios within convective updrafts, resulting in upper tropospheric ozone reductions of nearly 7 ppbv/day. This convective ozone sink is localized near the region of largest net photochemical production, suggesting lighting NOx emissions and convective transport of boundary layer NOx emissions play an important role in the upper tropospheric ozone production. Lateral detrainment of higher ozone mixing ratios during deep convection leads to midtropospheric increases in ozone at a rate of 5 ppbv/day. Shallow convection near 40°N results in entrainment of higher ozone mixing ratios associated with ozone production within the continental boundary layer. This low level entrainment and subsequent convective lofting leads to localized convectively induced ozone sinks of up to 2.0 ppbv/day in this region. The RMS effects of the ozone assimilation are less than 1% over much of the troposphere, with localized regions below 2 km in the northern part of the budget domain showing upward of 2% RMS changes. Relatively uniform assimilation increments of 2% or more are found just above the tropopause and are a result of the assimilation of the solar occultation and limb scattering measurements.

[38] Figure 14 shows the time averaged ozone number densities for each of the lateral boundaries of the continental U.S. domain. The time averaged altitudes of the tropopause and 380 K potential temperature surface are also shown. On the western boundary the ozone number densities are very low below 2 km, reflecting the influence of clean maritime air. Midtropospheric ozone enhancements are found along each domain boundaries. Within the middle world, there are local maxima in ozone number densities near the northern edges of both the western and eastern boundaries, as well as over the western half of the northern boundary. These local maxima are evidence for the accumulation of ozone within the middle world and are a result of the global-scale vertical and horizontal flux convergence poleward of the tropopause break discussed in section 4. The largest local enhancements in ozone number densities are found in the middle world along the western portion of the northern boundary. These ozone enhancements are associated with an upper tropo-spheric trough pattern which persisted during much of INTEX-A. The signature of this upper tropospheric trough is evident in the lower time averaged tropopause altitudes along the western portion of the northern boundary. Local enhancements in ozone number densities below 5 km along the northern boundary are the result of ozone production within the Alaskan and Canadian wild fire plumes.

[39] Figure 15 shows the time averaged ozone fluxes, in mol/cm^2/s, for each of the lateral boundaries of the conti-nental U.S. domain. Negative values denote fluxes into the continental United States while positive values denote export out of the continental United States. The largest ozone fluxes (both into and out of the continental United States) occur along the eastern and western boundaries and arise because of the prevailing westerly winds along the northern portion of the continental United States. These ozone fluxes maximize in the middle world, and are coincident with local maxima in ozone number densities shown in Figure 14. There is a reversal of the fluxes on the eastern and western boundaries over the southern United
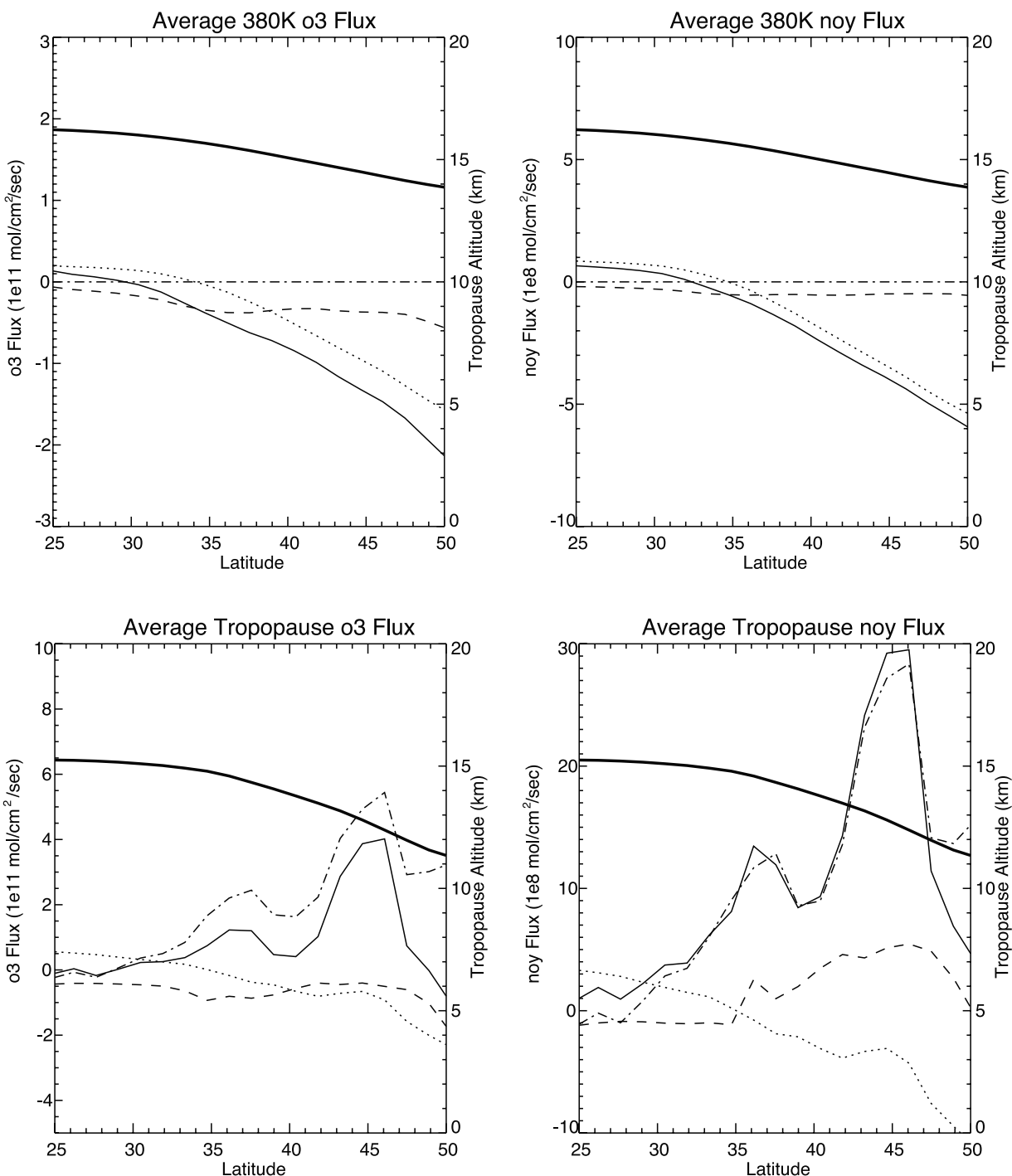
Figure 12. Zonally averaged continental U.S. (top) 380 K and (bottom) cross tropopause fluxes of (left) O3 (10^{11} mol/cm^2/s) and (right) NOy (10^8 mol/cm^2/s) during 1 July to 15 August 2004. The thin solid line is the net flux, which is the sum of isentropic (dash-dot), diabatic (dotted), and movement of the surface (dashed). The bold line denotes the mean altitude (km) of the 380 K and tropopause surface.

States associated with the prevailing stratospheric easterlies near 20 km. The ozone export along the eastern boundary is significantly larger than ozone import along the western boundary, leading to net ozone export out of the continental United States. The alternating pattern of middle world ozone fluxes along on the northern boundary is a consequence of meridional transport within the upper level trough, with net import on the western flank and export on the eastern flank. The ozone fluxes along the southern boundary are very small.

[40] The large time averaged lateral fluxes, coupled with flux convergence associated with upward STE and downward diabatic transport into the middle world, suggest that neglecting this region in the U.S. ozone budget could lead to significant underestimates in the actual export during INTEX-A. Consequently, in the subsequent budget analysis,
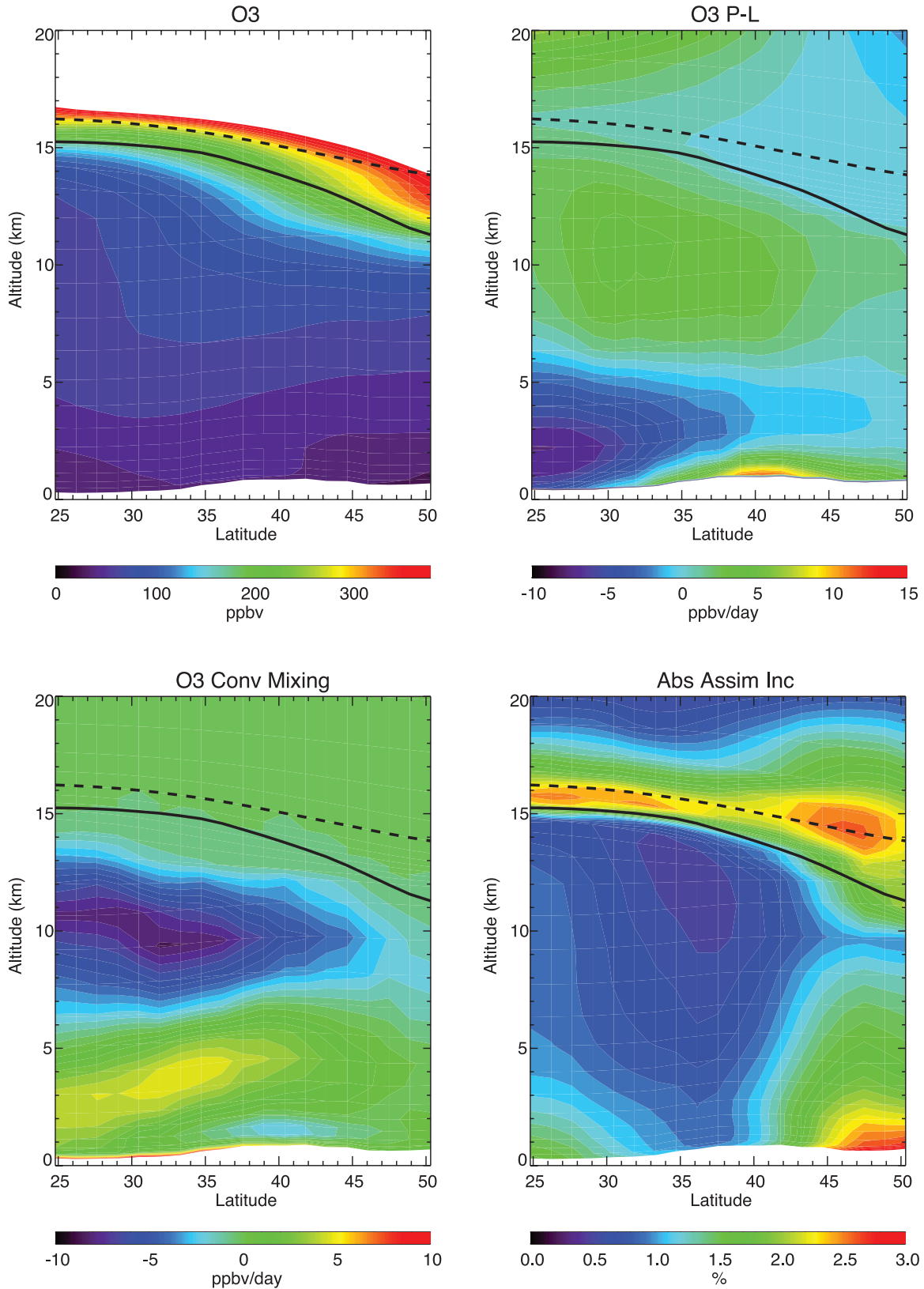
Figure 13. Time averaged zonal mean distribution of continental U.S. ozone (ppbv), net P-L (ppbv/day), convective mixing tendencies (ppbv/day) and absolute assimilation increment (%) as a function of altitude (km) and latitude within the continental U.S. budget domain during 1 July to 15 August 1004.
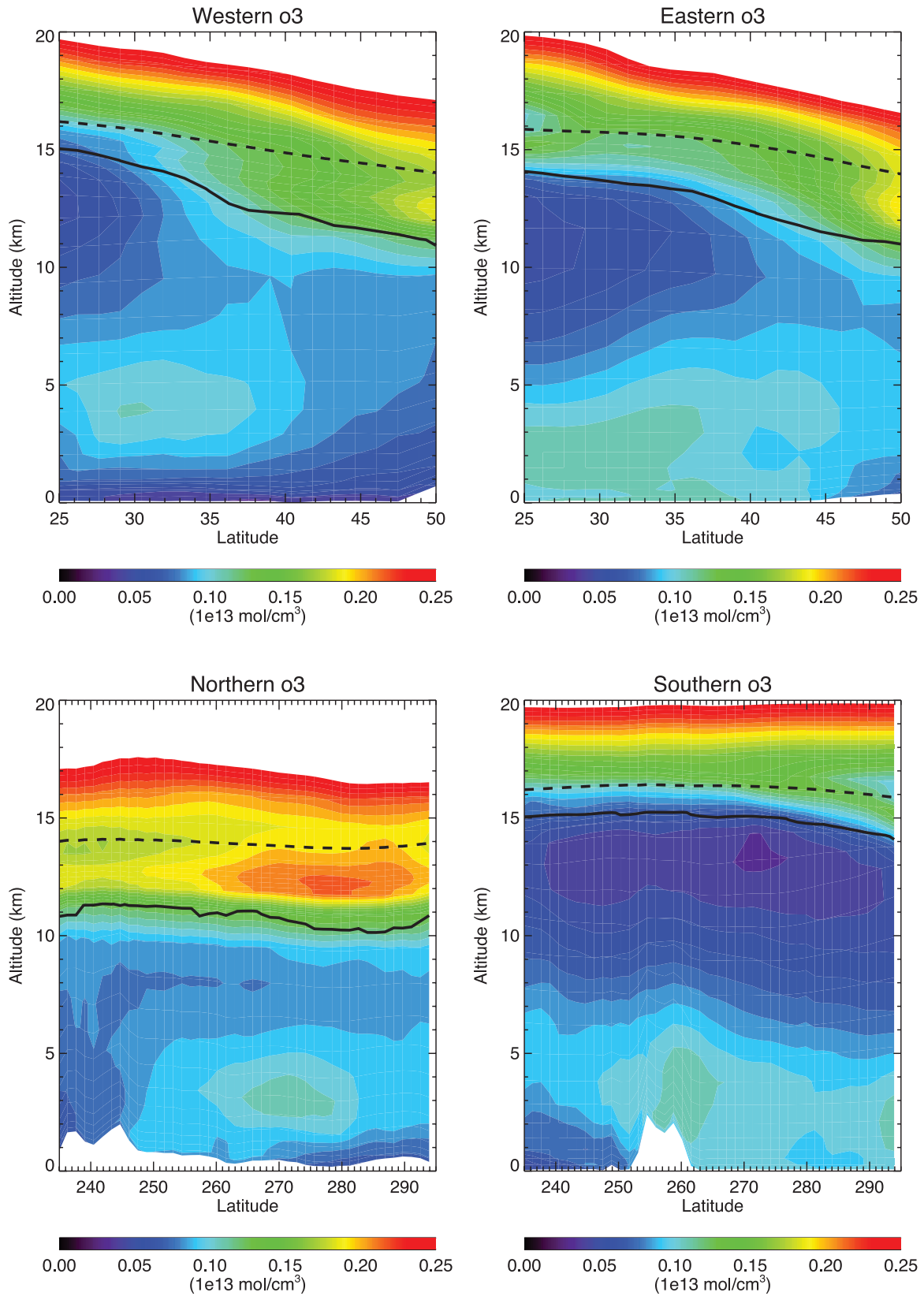
Figure 14. Time averaged ozone number densities (mol/cm^3) for each of the lateral boundaries of the continental U.S. budget domain for 1 July to 15 August 2004.
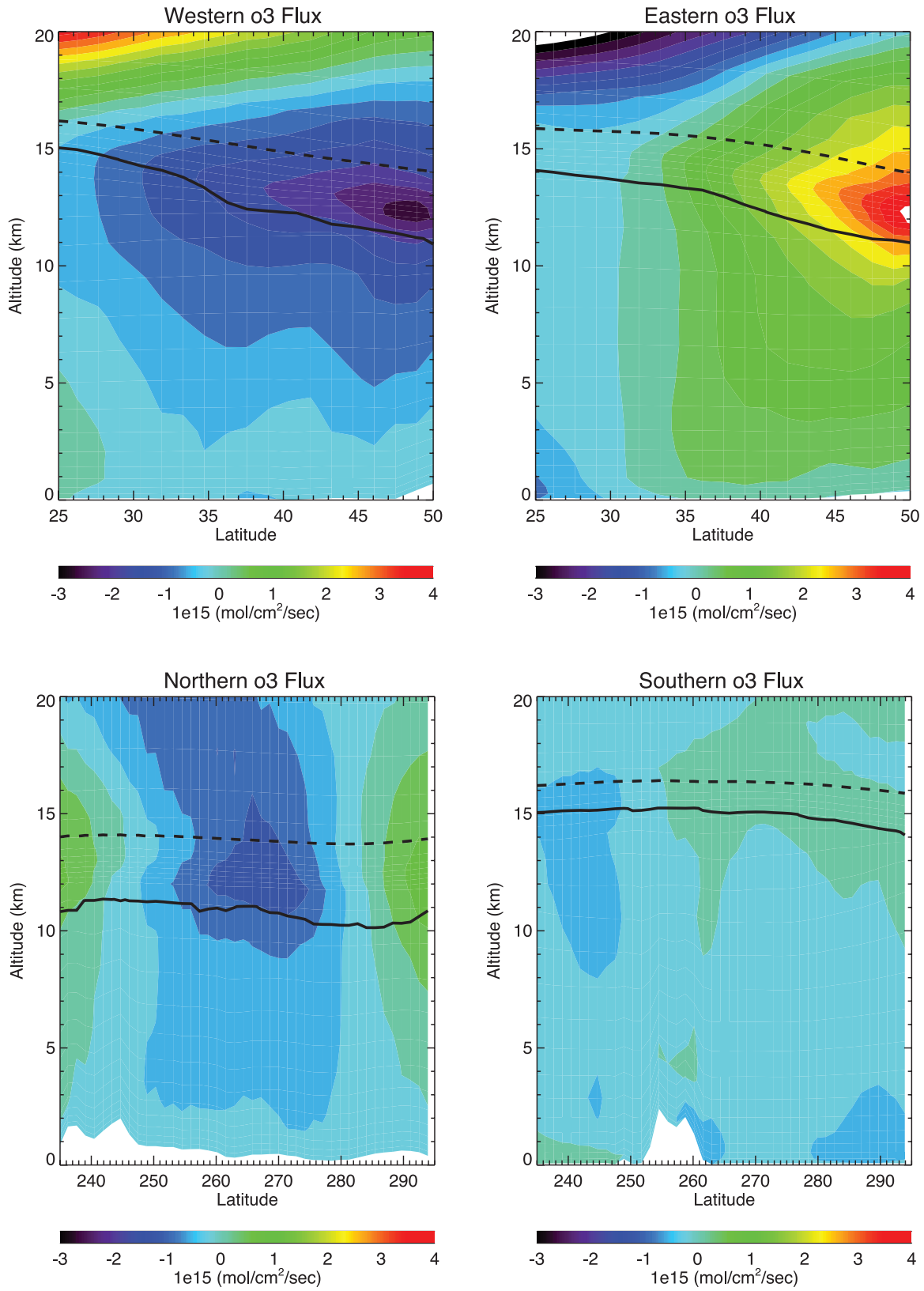
Figure 15. Time averaged ozone fluxes (mol/cm^2/s) for each of the lateral boundaries of the continental U.S. budget domain for 1 July to 15 August 2004. Negative fluxes are into the domain.
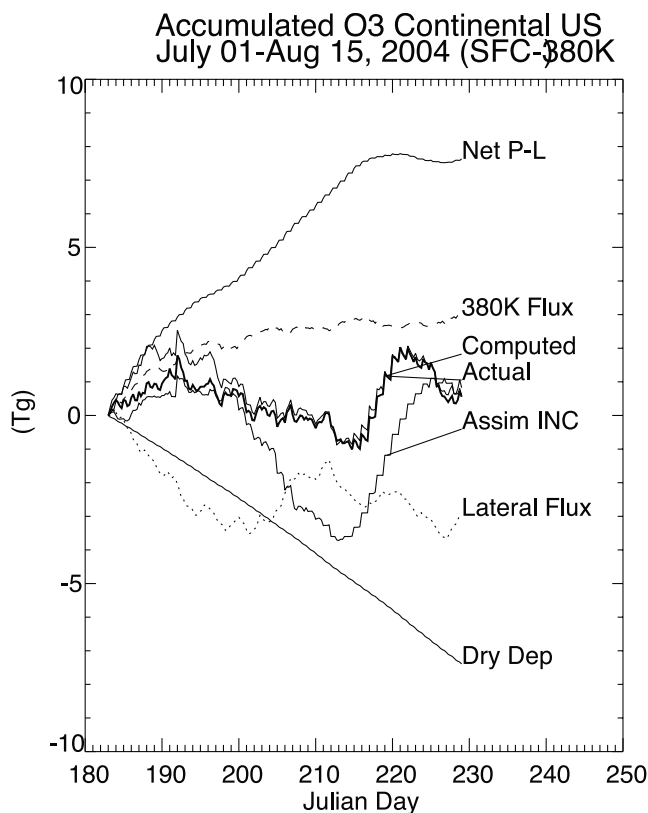
Figure 16. Time series of accumulated changes in continental U.S. ozone (Tg) for 1 July to 15 August 2004 due to P-L, 380 K fluxes, lateral fluxes, ozone assimilation, and dry deposition. The actual and computed accumulation is also shown.

we consider the 380 K potential temperature surface to be the top of the budget domain. Figure 16 shows the time series of the accumulated changes in continental U.S. ozone associated with ozone production, 380 K diabatic fluxes, lateral fluxes, ozone assimilation, and dry deposition. The actual and computed accumulation, determined from the sum of the individual budget terms, is also shown. The initial continental United States ozone burden below 380 K was 15.6 Tg. Variations in the total ozone below 380 K are on the order of 2 Tg with small (<1 Tg) net changes in continental U.S. ozone during INTEX-A. The close agreement between the actual and computed accumulation during INTEX-A indicates low accumulative errors in the budget calculation.

[41] Net photochemical production is the dominant source of changes in continental U.S. ozone during INTEX-A, with accumulated in situ ozone production of 7.63 Tg. However, photochemical production slows down significantly after Julian Day 198 (15 July), as reflected in the much slower accumulation due to ozone photochemistry during the later half of July, and becomes negative in August, as reflected in the decline in ozone accumulation due to net P-L after Julian day 220. The reductions in photochemical ozone production are attributed to the anomalously cold weather pattern during these periods. August 2004 was the 7th coldest on record with cold outbreaks occurring during 26–30 July and 10–16 August [*Fuelberg*

et al., 2007]. These cold air outbreaks are associated with increased surface winds which lead to efficient boundary layer ventilation and reduced accumulation of ozone precursors. U.S. EPA air quality statistics for 92 major metropolitan areas in the continental United States show that 2004 had the fewest days with ozone Air Quality Indexes over 100 (corresponding to 8 hour average ozone mixing ratios greater than 85 ppbv) during the last 15 years (1990–2004). The reduction was highly significant. When all U.S. metropolitan areas are considered the number of ozone AQI > 100 days in 2004 was 66% less than the 15 year median value. If we exclude California, Dallas, and Houston the number of ozone AQI > 100 days in 2004 was 82% less than the 15 year median.

[42] The rate of ozone loss due to dry deposition remains nearly constant throughout the INTEX-A period and is the dominate sink of ozone within the budget volume. Accumulated losses due to dry deposition (7.39 Tg) nearly balance net photochemical production over the continental United States during INTEX-A. Lateral ozone fluxes result in accumulative reductions (net export) of 3 Tg during INTEX-A, however, most of this export occurs prior to Julian Day 201 (18 July). After 18 July there were a series of anomalously deep upper level troughs over the United States [*Fuelberg et al.*, 2007] which contributed to the significant week to week variability in the lateral fluxes during the latter half of July and first half of August. Diabatic fluxes across the 380 K surface result in the import of 3 Tg of stratospheric ozone to the continental U.S. domain during the INTEX-A time period.

[43] There is a significant reduction in the rate of accumulation of stratospheric ozone within the continental U.S. domain after Julian day 197 (15 July) corresponding to the beginning of the assimilation of SAGE III limb scattering measurements. As was shown in section 3.2, assimilation of SAGE limb scattering measurements had a positive impact on the RAQMS versus IONS ozonesonde statistics by reducing high biases in the region of the upper troposphere with significant stratospheric influences. Assimilation increments during the SAGE limb scattering period (15–31 July) result in a net loss of 3 Tg of ozone over the continental United States, which is comparable in magnitude to the total ozone export during INTEX-A. After 31 July the assimilation of the SAGE limb scattering measurements stops and assimilation of TOMS column ozone only results in systematic increases in ozone within the budget volume until the SAGE limb scattering assimilation is resumed on 12 August. The assimilation of SAGE III limb scattering measurements also impacts the estimates of lateral fluxes, which maximize in the middle world. This is reflected in the anticorrelation between the accumulated effects of assimilation and lateral fluxes after 15 July. Whether changes in the lateral fluxes are associated with the inclusion of SAGE III limb scattering data in the assimilation or changes in the upper tropospheric circulation during the latter part of INTEX-A is a difficult question to answer. Future budget studies could address this question by conducting budget analysis with and without assimilation.

[44] The majority of the export from the continental U.S. domain occurs in the middle world, consequently, the net import of approximately 3 Tg of stratospheric ozone across the 380 K potential temperature surface is likely to account

for the majority of the 3 Tg of ozone that is exported during INTEX-A. To obtain an estimate of the export of ozone that was photochemically produced within the continental U.S. domain during INTEX-A we need to remove the stratospheric contribution from the accumulated lateral export. This results in 9.4e9 g of ozone photochemically produced over the United States and exported during INTEX-A, which is a negligible fraction of the total export.

5.2. NOy Budget Analysis

[45] The export of total reactive nitrogen (NOy) from the continental United States is equally as important as the export of ozone, since availability of nitrogen oxides (NO + NO$_2$) determine subsequent ozone production [*Chameides et al.*, 1992]. In this section we discuss results from Eulerian budget calculations focusing on NOy. Figure 17 shows the time averaged zonal mean distribution of continental United States NOy, lighting NOx production, convective exchange of NOy, and NOy wet deposition. The zonal mean surface NOy is over 4 ppbv and is dominated by localized NOx enhancements due to emissions and HNO3. There is a pronounced tongue of elevated NOy extending down from the midlatitude tropopause that has significant stratospheric influences. Since the cross tropopause NOy flux is from the troposphere to the stratosphere within the continental U.S. budget domain, these NOy enhancements must arise because of STE outside of the continental United States.

[46] Cloud top detrainment of lightning NOx emissions in the southern portion of the domain results in NOy production of 0.25 ppbv/day in the upper troposphere (7–10 km), with nearly equal amounts below 2 km associated with outflow from convective downdrafts [*Pickering et al.*, 1998]. Convective mixing entrains continental boundary layer NOy at a rate of 2 ppbv/day where it is either immediately rained out (for highly soluble species such as HNO3) or convectively lofted (for less soluble species such as PAN) and deposited between 5 and 10 km. In contrast to ozone, convective exchange increases free tropospheric NOy mixing ratios at a rate of 0.15 ppbv/day. This is a consequence of the different vertical gradients in NOy and ozone below 10 km.

[47] Figure 18 shows the time averaged NOy number densities for each of the lateral boundaries of the continental U.S. domain. The distribution of middle world NOy and ozone number densities (Figure 14) are very similar with local maxima on the northern edges of the western and eastern boundaries and on the eastern edge of the northern boundary. These local maxima are primarily HNO3, and result from net flux converge within this region. However, in the troposphere there are significant differences between the ozone and NOy number densities on the lateral boundaries. The largest NOy number densities are found below 5 km on the northern boundary and below 2 km on the eastern boundary. The enhancements in NOy on the northern boundary, which are coincident with ozone enhancements shown in Figure 14, are primarily HNO3 and PAN and are due to transport of emissions from the Alaskan wild fires. The large local enhancements in NOy number densities below 2 km along the eastern boundary are primarily due to HNO3 as are the low level enhancements in NOy on the western boundary. Midtropospheric enhancements in NOy number densities along the eastern and southern

boundaries are primarily due to PAN. Figure 19 shows the time averaged NOy fluxes, in mol/cm^2/s, for each of the lateral boundaries of the continental U.S. domain. As with the number densities, the distribution of NOy fluxes in the middle world are similar to the ozone fluxes (Figure 15) and are dominated by fluxes of HNO3. In the troposphere, there is significant NOy import (negative fluxes) on the northern boundary near 5 km. These fluxes are primarily due to transport of HNO3 and PAN from the Alaskan wildfires. The NOy export (positive fluxes) on the northern part of the eastern boundary extends well into the troposphere. This is due to export of PAN, which maximizes near 7 km along the northern portion of the eastern boundary. The localized export of NOy below 2 km at 45N is primarily composed of HNO3.

[48] While there is significant complexity in the way that NOy species are partitioned among the various regions of import and export the evolution of the accumulated changes in continental NOy is actually quite simple because of the fact that its primary source is surface emissions, which are held constant throughout the simulation. Figure 20 shows the time series of the accumulated changes in continental U.S. NOy (expressed in Tg of nitrogen) due to sources (industrial plus aircraft and soil emissions, lightning emissions), sinks (wet and dry deposition) and transport (380 K diabiatic fluxes and lateral fluxes). The actual and computed accumulation, determined from the sum of the individual budget terms, is also shown. The initial continental U.S. NOy burden below 380 K was 0.05 Tg. The actual and computed NOy accumulation over the continental United States were very small during INTEX-A, as are the 380 K diabatic fluxes. The continental U.S. NOy budget shows accumulated NOy emissions of 0.94 Tg nitrogen (with less than 20% due to lightning NOx production) and accumulated depositional loss of 0.69 Tg nitrogen (0.47 Tg wet, 0.202 dry), resulting in a net export of 0.23 Tg of nitrogen and an export efficiency of 24%.

6. Discussion

[49] *Liang et al.* [1998, hereinafter referred to as L98] used sensitivity experiments based on differences between two continental-scale photochemical model simulations (one with and one without U.S. NOx emissions) to estimate seasonally averaged fluxes of ozone and NOy. The summer season (JJA) ozone export from the continental U.S. boundary layer in the standard (with U.S. NOx) simulation was 1.8 Gmol/day, while difference between the standard simulation and one without U.S. NOx emissions, referred to as "pollution ozone" was 6.5 Gmol/day. *Li et al.* [2004, hereinafter referred to as L04] used the GEOS-CHEM model sensitivity experiments to estimate U.S. ozone export out of the continental U.S. boundary layer during September 1997 and found "pollution ozone" export of 5 Gmol/day, consistent with the fall (SON) estimates by L98. Furthermore, L04 showed that nearly 70% of the ozone production associated with continental U.S. NOy export out of the boundary layer occurs directly over North America, referred to as "near field ozone production," and would therefore be included in the RAQMS INTEX-A continental U.S. budget calculations presented here.
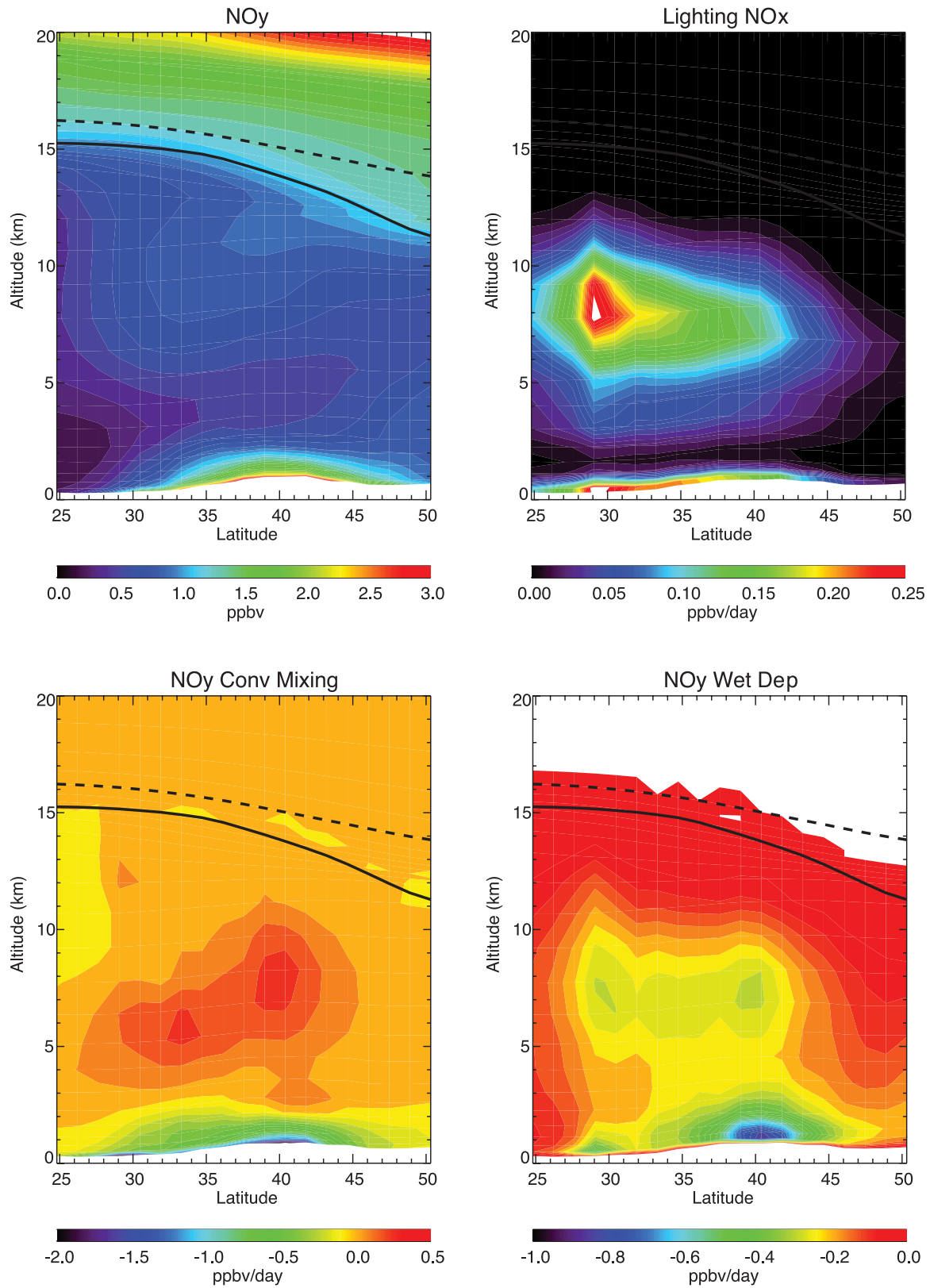
Figure 17. Time averaged zonal mean distribution of continental U.S. NOy (ppbv), net production due to lightning NOx (ppbv/day), convective mixing tendencies (ppbv/day) and wet deposition (ppbv/day) as a function of altitude (km) and latitude within the continental U.S. budget domain during 1 July to 15 August 1004.
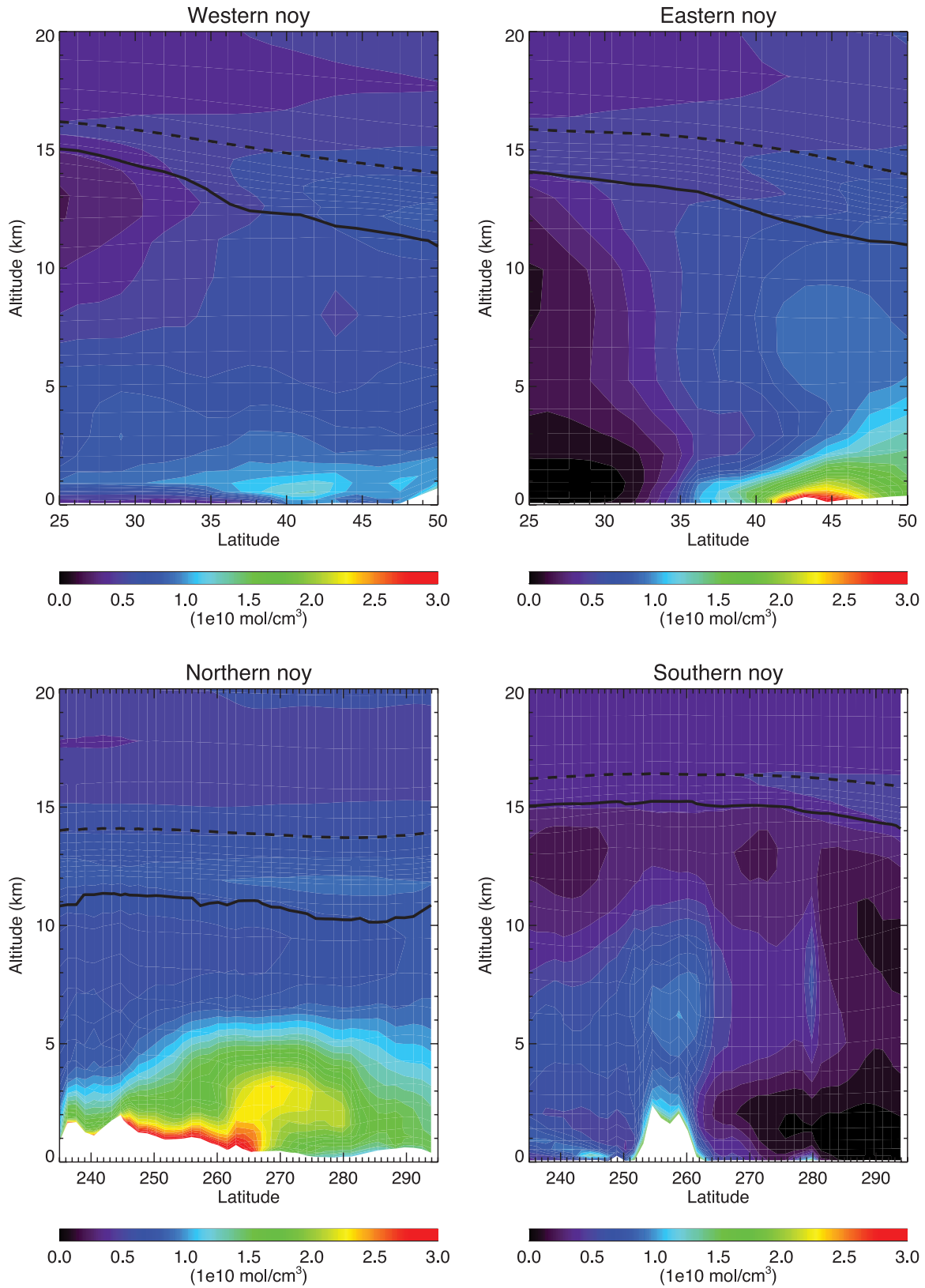
Figure 18. Time averaged NOy number densities (mol/cm^3) for each of the lateral boundaries of the continental U.S. budget domain for 1 July to 15 August 2004.
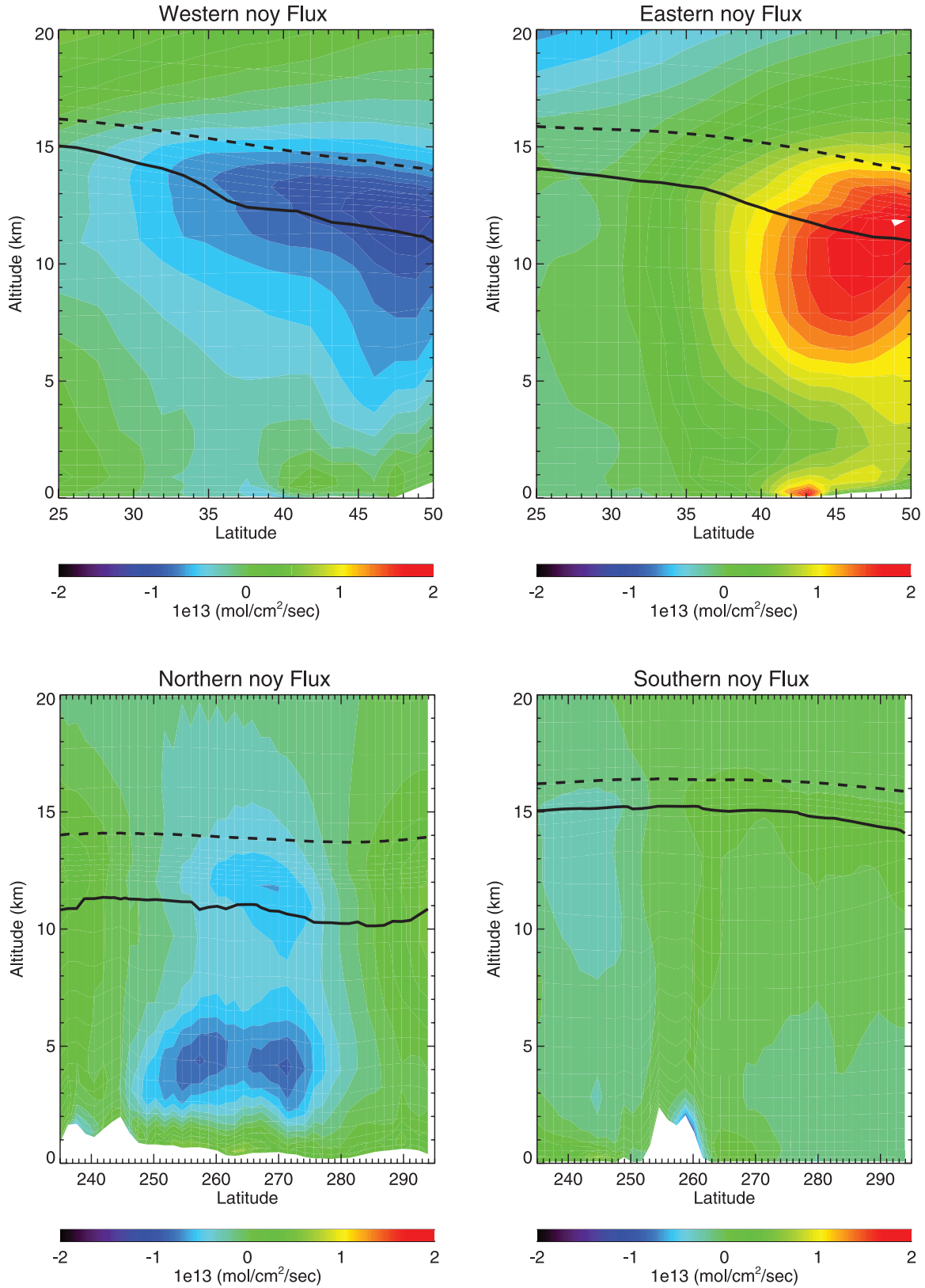
Figure 19. Time averaged ozone fluxes (mol/cm²/s) for each of the lateral boundaries of the continental U.S. budget domain for 1 July to 15 August 2004. Negative fluxes are into the domain.
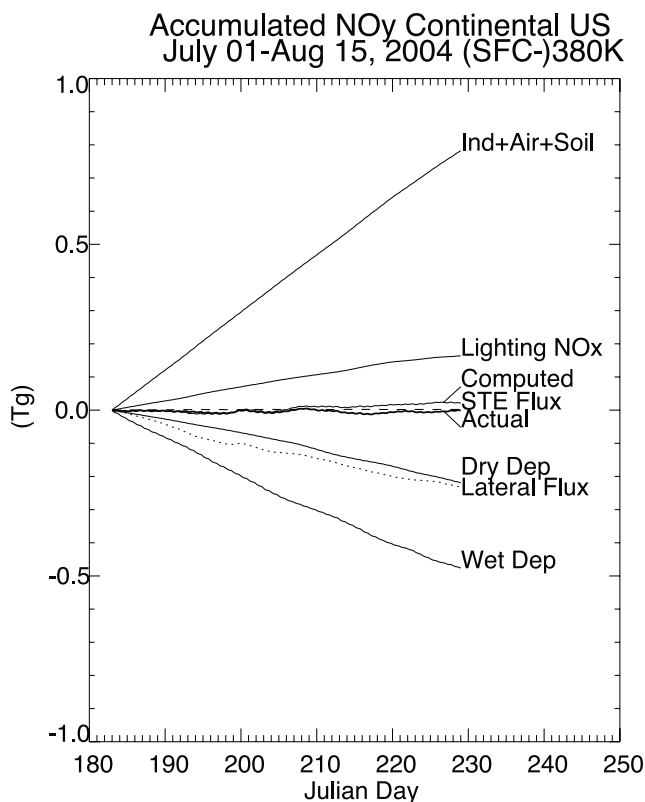
Figure 20. Time series of accumulated changes in continental U.S. NOy (Tg Nitrogen) for 1 July to 15 August 2004 due to emissions, 380 K fluxes, lateral fluxes, lightning NOx, and wet and dry deposition. The actual and computed accumulation is also shown.

[50] The L98 horizontal continental U.S. domain size was similar to the current INTEX-A budget domain. Applying the JJA L98 standard simulation export rate over the 46 day INTEX-A budget period would result in 3.97 Tg of ozone exported through the continental U.S. boundary layer, comparable to our estimates of net export, however, as discussed earlier, the RAQMS INTEX-A ozone export is of stratospheric origin. Applying the JJA L98 ''pollution ozone'' export rate over the 46 day INTEX-A budget period would result in 14.35 Tg of U.S. ozone exported through the continental boundary layer, which is significantly larger than our estimates of net export of photochemically produced ozone from the continental U.S. budget domain during INTEX-A.

[51] Direct comparisons of the INTEX-A continental U.S. photochemical ozone export and the L98 and L04 ''pollution ozone'' estimates are not appropriate since the ''pollution ozone'' reflects the fact that without emissions, the continental United States would be a strong sink of ozone due to photochemical losses and dry deposition near the surface. However, because of the large discrepancies between the L98 standard simulation and the RAQMS estimates of ozone export during INTEX-A, some discussion is warranted.

[52] The main reason for the large differences between the current estimate of U.S. photochemical ozone export during INTEX-A and the L98 standard simulations results is

the anomalously cold surface temperatures during August 2004, which actually resulted in net photochemical ozone loss within the continental U.S. domain during the first 2 weeks of August. If we restrict our budget calculations to 1–15 July, we obtain a net export of photochemically produced ozone of 1.4 Tg. This export is in good agreement with the ozone export that would be obtained by applying the L98 JJA seasonal rate of 1.8 Gmol/day from the standard simulation over this same period (1.3 Tg). However, the RAQMS ozone budget includes ozone production above the continental boundary layer while the L98 does not. The accumulated ozone P-L within the budget domain from July 1–15 is 3.84 Tg. This is 85% of the accumulated continental boundary layer P-L that would be obtained for the same 15 day period using seasonally averaged P-L rates from the L98 standard simulation. The RAQMS simulation removes 2.23 Tg, or 58% of the ozone produced over the continental United States due to dry deposition during the period from 1 to 15 July. In contrast, dry deposition removes only 33% of the ozone produced over the continental United States in the L98 standard simulation.

[53] As shown in section 3.3, the RAQMS estimates in P-L are in good agreement with observationally constrained photochemical box model estimates during INTEX-A, indicating that the current estimates of P-L are reasonable. *Talbot et al.* [2005] provide estimates of nocturnal ozone dry deposition during the summer based on 3 years (2001–2003) of ozone measurements at the Harvard Forest site. They find median nocturnal deposition rates of 11 ppbv/night, which are considered representative of heavily forested regions in New England. This estimate compares very well with median RAQMS nighttime (0000–1200 UT) averaged ozone deposition velocities over New England (11.29 ppbv/night) during INTEX-A.

[54] Taken as a whole, these comparisons indicate that the photochemical ozone export from the continental U.S. budget domain during 1–15 July 2004 was consistent with the L98 standard simulation results assuming that the near field ozone production due to NOy export through the continental U.S. boundary layer was small. However, because of anomalously cold surface temperatures and resulting net ozone destruction during the first two weeks of August, the export of photochemically produced ozone was insignificant compared to the export of stratospheric ozone in the upper troposphere/lower stratosphere over the continental United States during the overall INTEX-A time frame (1 July to 15 August 2004).

[55] The agreement between the RAQMS INTEX-A and J98 based estimates of continental U.S. NOy export over the INTEX-A time frame is quite good. Recall that the INTEX-A continental U.S. NOy budget shows accumulated NOy emissions of 0.94 Tg nitrogen and accumulated depositional loss of 0.69 Tg nitrogen (0.47 Tg wet, 0.202 dry), resulting in a net export of 0.23 Tg of nitrogen and an export efficiency of 24%. Applying the rates from L98 NOy budget estimates to the INTEX-A time period results in 0.86 Tg of nitrogen emissions, accumulated depositional loss of 0.64 Tg nitrogen (0.24 Tg wet, 0.4 dry), net export of 0.23 Tg of nitrogen and an export efficiency of 27%, all of which are within 10% or less of the INTEX-A estimates. Wet deposition accounts for the majority of the NOy depositional loss based on the RAQMS budget calculations

where as dry deposition accounts for the majority of the L98 depositional loss. This is to be expected since the RAQMS budget domain includes the entire troposphere and consequently the full vertical extent of wet deposition within convective cells is included in the NOy budget. The RAQMS budget analysis indicates that NOx+PAN accounts for 54% of the NOy exported out of the continental United States during INTEX-A, which is 15% lower than the L98 estimate of 63%. This difference is due to the additional contributions from HNO3 export in the middle world which is included in the RAQMS NOy budget calculations. Both INTEX-A and J1998 export efficiencies are slightly higher than the L04 Eulerian estimates of 20% during September 1997. The RAQMS Eulerian estimates of export efficiency are slightly higher than obtained by *Hudman et al.* [2007] using Lagrangian NOy-CO correlations from GEOS-CHEM (14 ± 8%) and P3 measurements (16 ± 10%) although still within the estimated range of uncertainty.

7. Summary and Conclusions

[56] We have used aircraft, satellite, surface, and ozonesonde measurements to assess the fidelity a 6 week RAQMS simulation of the unified troposphere-stratosphere chemistry during the INTEX-A time period. These comparisons show that RAQMS captures the main features of the global tropospheric distribution of ozone, carbon monoxide, and NO2 with reasonable fidelity, although RAQMS underestimates the median tropospheric NO2 distribution relative to SCIAMACHY measurements and overestimates the impact of the Alaskan wild fires on column CO relative to MOPITT.

[57] Comparisons with in situ airborne measurements shows that RAQMS reproduces the statistical characteristics of the in situ observations (median and variances) with reasonable accuracy (generally within 20%) although RAQMS tends to overestimate stratospheric influences and underestimate convective influences in the upper troposphere. Comparisons with in situ airborne measurements also shows that RAQMS overestimates wet deposition (low biases in NOy and HNO3 below 600 mbar) in the lower troposphere. Comparisons with P3 measurements shows that RAQMS NO2 predictions are in good agreement with in situ measurements in the NE United States while comparisons with DC8 measurements shows that RAQMS tends to overestimate boundary layer NO2 over more rural regions of the eastern United States. The in situ NO2 comparisons point to an apparent discrepancy between satellite-based tropospheric NO2 columns and median NO2 column estimates from the in situ statistics. This discrepancy warrants further investigation and may be due to contributions the NO2 column from below the minimum altitudes of the DC8 and P3 or biases in the satellite retrieval.

[58] On the basis of comparisons with ozonesondes from the IONS network, the assimilation of satellite-based profile and column ozone measurements has been shown to have a positive impact on the RAQMS upper tropospheric/lower stratosphere ozone analyses (mean biases of 20%), particularly during the period when higher density SAGE III limb scattering measurements were available over the continental United States. Comparisons with surface ozone measurements from the U.S. EPA AIRNOW network show that the RAQMS surface ozone analysis captures the daily variability in surface ozone over most of the eastern United States very well, with correlations between 24 hour averaged measurements and the RAQMS analysis generally near 0.8. However, because of local variations in topography and emissions, the daily correlations over the central Appalachians are considerably lower (0.2–0.4). The RAQMS surface ozone analysis shows a systematic high bias (18 ppbv at night, 15 ppbv during the day) relative to AIRNow surface measurements, which is attributed to underestimates in nocturnal titration due to underestimates of surface NOx in urban environments. Improper representation of mixing processes within the nocturnal boundary layer in urban regions may also contribute to the systematic nighttime high biases.

[59] Eulerian ozone and NOy budgets during INTEX-A show that the majority of the continental U.S. export during INTEX-A occurred in the upper troposphere/lower stratosphere poleward of the tropopause break. The localized ozone and NOy export was shown to occur because of convergence of tropospheric and stratospheric air in this region. These results suggest that providing a robust assessment of the influence of the continental United States on the global environment requires accurate representation of the long-range transport and mixing processes within this region. Continental U.S. photochemically produced ozone was found to be a minor component of the total ozone export, which was dominated by stratospheric ozone that was diabatically transported into the middle world during INTEX-A. The unusually low photochemical ozone export is attributed to anomalously cold surface temperatures during the latter half of the INTEX-A mission. Efficient boundary layer venting associated with cold air outbreaks during late July and mid-August tended to reduce accumulation of ozone precursors resulting in net ozone loss during the first 2 weeks of August.

[60] Eulerian NOy budgets during INTEX-A where shown to be very consistent with previously published model-based estimates. The NOy export efficiency was estimated to be 24%, with NOx + PAN accounting for 54% of the total NOy export during INTEX-A. However, the RAQMS estimates of export efficiency should be considered in light of the 30–40% low bias in NOy and HNO3 below 600 mbar relative to P3 and DC8 in situ measurements, which results in lower computed export efficiencies due to reductions in the predicted HNO3.

References

Atherton, C. S., et al. (1996), Three-dimensional global modeling studies of the transport and photochemistry over the North Atlantic Ocean, *J. Geophys. Res.*, *101*, 29,289–29,304.

Bertram, T. H., A. Heckel, A. Richter, J. P. Burrows, and R. C. Cohen (2005), Satellite measurements of daily variations in soil NO_x emissions, *Geophys. Res. Lett.*, *32*, L24812, doi:10.1029/2005GL024640.

Bian, H., and M. J. Prather (2002), Fast-J2 accurate simulation of stratospheric photolysis in global chemical models, *J. Atmos. Chem.*, *41*, 281–296.

Carslaw, K. S., B. Luo, and T. Peter (1995), An analytic expression for the composition of aqueous HNO_3-H_2SO_4 stratospheric aerosols including gas phase removal of HNO_3, *Geophys. Res. Lett.*, *22*(14), 1877–1880.

Carter, W. (1996), Condensed atmospheric photooxidation mechanisms for isoprene, *Atmos. Environ.*, *30*, 4275–4290.

Chameides, W. L., et al. (1992), Ozone precursor relationships in the ambient atmosphere, *J. Geophys. Res.*, *97*, 6037–6055.

Chipperfield, M. P. (1999), Multiannual simulations with a three-dimensional chemical transport model, *J. Geophys. Res.*, *104*(D1), 1781–1806.

Cofer, W. R., III, E. L. Winstead, B. J. Stocks, D. R. Cahoon, J. G. Goldammer, and J. S. Levine (1996a), Composition of smoke from North American boreal forest fires, in *Fire in Ecosystems of Boreal Eurasia,* edited by J. G. Goldammer and V. V. Furyaev, pp. 465–475, Kluwer Acad., Dordrecht, Netherlands.

Cofer, W. R., III, E. L. Winstead, B. J. Stocks, L. W. Overbay, J. G. Goldammer, D. R. Cahoon Jr., and J. S. Levine (1996b), Emissions from boreal forest fires: Are the atmospheric impacts underestimated?, in *Biomass Burning and Global Change,* edited by J. S. Levine, pp. 834–839, MIT Press, Cambridge, Mass.

Dentener, F. J., and P. J. Crutzen (1993), Reaction of N_2O_5 on tropospheric aerosols: Impact on the global distributions of NO_x, O_3 and OH, *J. Geophys. Res.*, *98*, 7149–7163.

Duncan, B. N., and I. Bey (2004), A modeling study of the export pathways of pollution from Europe: Seasonal and interannual variations (1987–1997), *J. Geophys. Res.*, *109*, D08301, doi:10.1029/2003JD004079.

Errico, R. M. (1999), Meeting summary, Workshop on Assimilation of Satellite Data, *Bull. Am. Meteorol. Soc.*, *80*, 463–471.

Fairlie, T. D., et al. (2007), Impact of multiscale dynamical processes and mixing on the chemical composition of the upper troposphere and lower stratosphere during INTEX-A, *J. Geophys. Res.*, doi:10.1029/2006JD007923, in press.

Fehsenfeld, F. C., et al. (2006), International Consortium for Atmospheric Research on Transport and Transformation (ICARTT): North America to Europe—Overview of the 004 summer field study, *J. Geophys. Res.*, *111*, D23S01, doi:10.1029/2006JD007829.

Fishman, J., and A. E. Balok (1999), Calculation of daily tropospheric ozone residuals using TOMS and empirically improved SBUV measurements: Application to an ozone pollution episode over the eastern United States, *J. Geophys. Res.*, *104*, 30,319–30,340.

Fuelberg, H. E., M. J. Porter, C. M. Kiley, J. J. Halland, and D. Morse (2007), Meteorological conditions and anomalies during the Intercontinental Chemical Transport Experiment-North America, *J. Geophys. Res.*, *112*, D12S06, doi:10.1029/2006JD007734.

Galbally, I. E., and C. R. Roy (1980), Destruction of ozone at the Earths' surface, *Q. J. R. Meteorol. Soc.*, *106*, 599–620.

Gery, M. W., G. Z. Whitten, J. P. Killus, and M. C. Dodge (1989), A photochemical kinetics mechanism for urban and regional scale computer modeling, *J. Geophys. Res.*, *94*, 12,925–12,956.

Holton, J. R., P. H. Haynes, M. E. McIntyre, A. R. Douglass, R. B. Rood, and L. Pfister (1995), Stratosphere-troposphere exchange, *Rev. Geophys*, *33*(4), 403–440.

Horowitz, L. W., J. Liang, G. M. Gardner, and D. J. Jacob (1998), Export of reactive nitrogen from North America during summertime: Sensitivity to hydrocarbon chemistry, *J. Geophys. Res.*, *103*, 13,451–13,476.

Hudman, R. C., et al. (2007), Surface and lightning sources of nitrogen oxides over the United States: Magnitudes, chemical evolution, and outflow, *J. Geophys. Res.*, *112*, D12S05, doi:10.1029/2006JD007912.

Jacob, D. J., et al. (1993), Factors regulating ozone over the United States and its export to the global atmosphere, *J. Geophys. Res.*, *98*, 14,817–14,826.

Jaegle, L., L. Steinberger, R. V. Martin, and K. Chance (2005), Global partitioning of NO_x sources using satellite observations: Relative roles of fossil fuel combustion, biomass burning and soil emissions, *Faraday Disc.*, *130*, 407–423, doi:10.1039/b502128f.

Jeuken, A. B. M., H. J. Eskes, P. F. J. van Velthoven, H. M. Kelder, and E. V. Hólm (1999), Assimilation of total ozone satellite measurements in a three-dimensional tracer transport model, *J. Geophys. Res.*, *104*, 5551–5563.

Jing, P., D. M. Cunnold, H. J. Wang, and E.-S. Yang (2004), Isentropic cross-tropopause ozone transport in the Northern Hemisphere, *J. Atmos. Sci.*, *61*, 1068–1078.

Kasibhatla, P. S., H. Levy III, and W. J. Moxim (1993), Global NO_x, HNO_3, PAN, and NO_y distributions from fossil fuel combustion emissions: A model study, *J. Geophys. Res.*, *98*, 7165–7180.

Kiley, C. M., et al. (2003), An intercomparison and evaluation of aircraft-derived and simulated CO from seven chemical transport models during the TRACE-P experiment, *J. Geophys. Res.*, *108*(D21), 8819, doi:10.1029/2002JD003089.

Kirchner, F., and W. R. Stockwell (1996), Effect of peroxy radical reactions on the predicted concentrations of ozone, nitrogenous compounds, and radicals, *J. Geophys. Res.*, *101*(D15), 21,007–21,022.

Knapp, K. G., et al. (1998), Observation of the transport of polluted air masses from the northeastern United States to Cape Sable Island, Nova Scotia, Canada, during the 1993 NARE summer intensive, *J. Geophys. Res.*, *103*, 13,399–13,411.

Lamarque, J. F., et al. (1999), Assimilation of Measurement of Air Pollution from Space (MAPS) CO in a global three-dimensional model, *J. Geophys. Res.*, *104*, 26,209–26,218.

Levy, H., II, J. D. Mahlman, W. J. Moxim, and S. C. Liu (1985), Tropospheric ozone: The role of transport, *J. Geophys. Res.*, *90*, 3735–3772.

Li, Q., D. J. Jacob, J. W. Munger, R. M. Yantosca, and D. D. Parrish (2004), Export of NO_y from the North American boundary layer: Reconciling aircraft observations and global model budgets, *J. Geophys. Res.*, *109*, D02313, doi:10.1029/2003JD004086.

Liang, J., et al. (1998), Seasonal budgets of reactive nitrogen species and ozone over the United States, and export fluxes to the global atmosphere, *J. Geophys. Res.*, *103*, 13,435–13,450.

Liu, H., D. J. Jacob, I. Bey, and R. M. Yantosca (2001), Constraints from ^{210}Pb and ^{7}Be on wet deposition and transport in a global three-dimensional chemical tracer model driven by assimilated meteorological fields, *J. Geophys. Res.*, *106*(D11), 12,109–12,128.

Martin, R. V., et al. (2002), An improved retrieval of tropospheric nitrogen dioxide from GOME, *J. Geophys. Res.*, *107*(D20), 4437, doi:10.1029/2001JD001027.

Martin, R. V., C. E. Sioris, K. Chance, T. B. Ryerson, T. H. Bertram, P. J. Wooldridge, R. C. Cohen, J. A. Neuman, A. Swanson, and F. M. Flocke (2006), Evaluation of space-based constraints on global nitrogen oxide emissions with regional aircraft measurements over and downwind of eastern North America, *J. Geophys. Res.*, *111*, D15308, doi:10.1029/2005JD006680.

McKeen, S., et al. (2005), Asessment of an ensemble of seven real-time ozone forecasts over eastern North America during summer 2004, *J. Geophys. Res.*, *110*, D21307, doi:10.1029/2005JD005858.

Muller, J. F., and G. Brasseur (1995), IMAGES: A three dimensional chemical transport model of the global troposphere, *J. Geophys. Res.*, *100*, 16,445–16,490.

Olson, J. R., J. H. Crawford, G. Chen, W. H. Brune, I. C. Faloona, D. Tan, H. Harder, and M. Martinez (2006), A reevaluation of airborne HO_x observations from NASA field campaigns, *J. Geophys. Res.*, *111*, D10301, doi:10.1029/2005JD006617.

Olson, J. S. (1983), Carbon in live vegetation of major world ecosystems, *ORNL-5862, Environ. Sci. Div. Publ. 1997,* Oak Ridge Natl. Lab., Oak Ridge, Tenn.

Oppenheim, A., and R. Schafer (1975), *Digital Signal Processing,* 585 pp. Prentice-Hall, Upper Saddle River, N. J.

Orlando, J. J., et al. (2002), Rate coefficient for the reaction of OH with CH2 = C (CH3)C (O)OONO2 (MPAN), *Atmos. Environ.*, *36*, 1895–1900.

Park, R. J., D. J. Jacob, B. D. Field, R. M. Yantosca, and M. Chin (2004), Natural and transboundary pollution influences on sulfate-nitrate-ammonium aerosols in the United States: Implications for policy, *J. Geophys. Res.*, *109*, D15204, doi:10.1029/2003JD004473.

Parrish, D. D., et al. (2004), Fraction and composition of NO_y transported in air masses lofted from the North American continental boundary layer, *J. Geophys. Res.*, *109*, D09302, doi:10.1029/2003JD004226.

Pfister, G., P. G. Hess, L. K. Emmons, J.-F. Lamarque, C. Wiedinmyer, D. P. Edwards, G. Pétron, J. C. Gille, and G. W. Sachse (2005), Quantifying CO emissions from the 2004 Alaskan wildfires using MOPITT CO data, *Geophys. Res. Lett.*, *32*, L11809, doi:10.1029/2005GL022995.

Pickering, K. E., Y. Wang, W.-K. Tao, C. Price, and J. F. Müller (1998), Vertical distributions of lightning NO_x for use in regional and global chemical transport models, *J. Geophys. Res.*, *103*(D23), 31,203–31,216.

Pierce, R. B., et al. (2003), Regional Air Quality Modeling System (RAQMS) predictions of the tropospheric ozone budget over east Asia, *J. Geophys. Res.*, *108*(D21), 8825, doi:10.1029/2002JD003176.

Price, C., J. Penner, and M. Prather (1997), NO_x from lightning: 1. Global distribution based on lightning physics, *J. Geophys. Res.*, *102*(D5), 5929–5942.

Rault, D. F. (2005), Ozone profile retrieval from SAGE III limb scatter measurements, *J. Geophys. Res.*, *110*, D09309, doi:10.1029/2004JD004970.

Rault, D. F., and G. Taha (2007), Validation of ozone profiles retrieved from Stratospheric Aerosol and Gas Experiment III limb scatter measurements, *J. Geophys. Res.*, doi:10.1029/2006JD007679, in press.

Ravishankara, A. R., E. J. Dunlea, M. A. Blitz, T. J. Dillon, D. E. Heard, M. J. Pilling, R. S. Strekowski, J. M. Nicovich, and P. H. Wine (2002), Redetermination of the rate coefficient for the reaction of O(^{1}D) with N_2, *Geophys. Res. Lett.*, *29*(15), 1745, doi:10.1029/2002GL014850.

Sander, S. P., R. R. Friedl, D. M. Golden, M. J. Kurylo, R. E. Huie, V. L. Orkin, A. R. Ravishankara, C. E. Kolb, and M. J. Molina (2003), Chemical kinetics and photochemical data for use in atmospheric studies, evaluation number 14, NASA Jet Propul. Lab., Calif. Inst. of Technol., Pasadena.

Savijarvi, H. (1995), Error growth in a large numerical forecast system, *Mon. Weather Rev.*, *123*, 212–221.

Schaack, T. K., T. H. Zapotocny, A. J. Lenzen, and D. R. Johnson (2004), Global climate simulation with the University of Wisconsin global hybrid isentropic coordinate model, *J. Clim.*, *17*, 2998–3016.

Schoeberl, M. R. (2004), Extratropical stratosphere-troposphere mass exchange, *J. Geophys. Res.*, *109*, D13303, doi:10.1029/2004JD004525.

Singh, H. B., W. H. Brune, J. H. Crawford, D. J. Jacob, and P. B. Russell (2006), Overview of the summer 2004 Intercontinental Chemical Transport Experiment-North America (INTEX-A), *J. Geophys. Res.*, *111*, D24S01, doi:10.1029/2006JD007905.

Soja, A. J., W. R. Cofer, H. H. Shugart, A. I. Sukhinin, P. W. Stackhouse Jr., D. J. McRae, and S. G. Conard (2004), Estimating fire emissions and disparities in boreal Siberia (1998–2002), *J. Geophys. Res.*, *109*, D14S06, doi:10.1029/2004JD004570.

Stajner, I., N. Winslow, R. B. Rood, and S. Pawson (2004), Monitoring of observation errors in the assimilation of satellite ozone data, *J. Geophys. Res.*, *109*, D06309, doi:10.1029/2003JD004118.

Stevenson, D. S., et al. (2006), Multimodel ensemble simulations of present-day and near-future tropospheric ozone, *J. Geophys. Res.*, *111*, D08301, doi:10.1029/2005JD006338.

Stobie, J. M. (1985), The use of optimum interpolation at AFGWC, paper presented at 7th Conference on Numerical Weather Prediction, Am. Meteorol. Soc., Montreal, Que., Canada.

Stobie, J. M. (2000), Algorithm theoretical basis document for statistical digital filter (SDF) analysis system (stretch-grid version), Data Assim. Off., NASA Goddard Space Flight Cent., Greenbelt, Md.

Stolarski, R. S., et al. (1995), Scientific assessment of the atmospheric effects of stratospheric aircraft, *NASA Ref. 1381*.

Streets, D. G., et al. (2003), An inventory of gaseous and primary aerosol emissions in Asia in the year 2000, *J. Geophys. Res.*, *108*(D21), 8809, doi:10.1029/2002JD003093.

Talbot, R., H. Mao, and B. Sive (2005), Diurnal characteristics of surface level O_3 and other important trace gases in New England, *J. Geophys. Res.*, *110*, D09307, doi:10.1029/2004JD005449.

Thompson, A. M., et al. (2007a), Intercontinental Chemical Transport Experiment Ozonesonde Network Study (IONS) 2004: 1. Summertime upper troposphere/lower stratosphere ozone over northeastern North America, *J. Geophys. Res.*, *112*, D12S12, doi:10.1029/2006JD007441.

Thompson, A. M., et al. (2007b), Intercontinental Chemical Transport Experiment Ozonesonde Network Study (IONS) 2004: 2. Tropospheric ozone budgets and variability over northeastern North America, *J. Geophys. Res.*, *112*, D12S13, doi:10.1029/2006JD007670.

Vose, J. M., W. T. Swank, C. D. Geron, and A. E. Major (1996), Emissions from forest burning in the southeastern United States: Application of a model determining spatial and temporal fire variation, in *Biomass Burning and Global Change*, edited by J. S. Levine, pp. 733–749, MIT Press, Cambridge, Mass.

Warneke, C., et al. (2006), Biomass burning and anthropogenic sources of CO over New England in the summer 2004, *J. Geophys. Res.*, *111*, D23S15, doi:10.1029/2005JD006878.

Wayland, R. A., et al. (2002), Communicating real-time and forecasted air quality to the public, *Environ. Manage.*, *30*(6), 28–36.

Wild, O., et al. (1996), Photochemical trajectory modeling studies of the North Atlantic region during August 1993, *J. Geophys. Res.*, *101*, 29,269–29,288.

World Meteorological Organization (1993), Scientific assessment of ozone depletion: 1991, *WMO Rep. 25*, Geneva, Switzerland.

Zapotocny, T. H., A. J. Lenzen, D. R. Johnson, F. M. Reames, P. A. Politowicz, and T. K. Schaack (1996), Joint distributions of potential vorticity and inert trace constituent in CCM2 and UW isentropic-sigma model simulations, *Geophys. Res. Lett.*, *23*, 2525–2528.

Zapotocny, T. H., A. J. Lenzen, D. R. Johnson, F. M. Reames, and T. K. Schaack (1997a), A comparison of inert trace constituent transport between the University of Wisconsin isentropic-sigma model and the NCAR community climate model, *Mon. Weather Rev.*, *125*, 120–142.

Zapotocny, T. H., D. R. Johnson, T. K. Schaack, A. J. Lenzen, F. M. Reames, and P. A. Politowicz (1997b), Simulations of joint distributions of equivalent potential temperature and an inert trace constituent in the UW isentropic-sigma model and CCM2, *Geophys. Res. Lett.*, *24*, 865–868.

Zaveri, R. A., and L. K. Peters (1999), A new lumped structure photochemical mechanism for large-scale applications, *J. Geophys. Res.*, *104*, 30,387–30,415.

Zinke, P. J., A. G. Strangenberger, W. M. Post, W. R. Emanuel, and J. S. Olson (1986), Worldwide organic soil carbon and nitrogen data, *NDP-018*, 134 pp., Oak Ridge Natl. Lab., Oak Ridge, Tenn.

———————————

J. A. Al-Saadi, M. A. Avery, J. Crawford, T. D. Fairlie J. Fishman, C. Kittaka, G. Lingenfelser, M. Natarajan, J. Olson, R. B. Pierce, D. Rault, G. W. Sachse, and A. Soja, NASA Langley Research Center, Hampton, VA 23681, USA. (j.a.al-saadi@nasa.gov; m.a.avery@larc.nasa.gov; j.h.crawford@larc.nasa.gov; t.d.fairlie@larc.nasa.gov; j.fishman@larc. nasa.gov; fn.c.kittaka@larc.nasa.gov; g.s.lingenfelser@larc.nasa.gov; m.natarajan@larc.nasa.gov; j.r.olson@larc.nasa.gov; r.b.pierce@larc.nasa. gov; d.f.rault@larc.nasa.gov; g.w.sachse@larc.nasa.gov; a.j.soja@larc. nasa.gov)

R. Cohen, Department of Chemistry, University of California, Berkeley, CA 94720-1640, USA. (cohen@cchem.berkeley.edu)

J. E. Dibb, Earth Sciences Department, University of New Hampshire Durham, NH 03824, USA. (jack.dibb@unh.edu)

D. Johnson, A. Lenzen, T. Schaack, and T. Zapotocny, Space Science and Engineering Center, University of Wisconsin, Madison, WI 53706, USA. (donj@ssec.wisc.edu; allenl@ssec.wisc.edu; todds@ssec.wisc.edu; tomz@ssec.wisc.edu)

R. Martin, Department of Physics and Atmospheric Science, Dalhousie University, Halifax, NS, Canada, B3H 4R2. (randall.martin@dal.ca)

J. Stobie, Science Applications International Corporation, Washington, DC 20591, USA. (james.stobie@auatac.com)

J. Szykman, NASA Langley Research Center, Hampton, VA 23681, USA. (j.j.szykman@larc.nasa.gov)

A. Thompson, Department of Meteorology, Pennsylvania State University, University Park, PA 16802, USA. (anne@met.psu.edu)